# Radiometer Design Analysis Based Upon Measurement Uncertainty

***Paul Racette*[1] *and Roger H. Lang*[2]**

[1]NASA Goddard Space Flight Center, Greenbelt, MD

Email: Paul.E.Racette@nasa.gov

[2]The George Washington University, Washington D.C.

Email: lang@gwu.edu

***Abstract*** - This paper introduces a method for predicting the performance of a radiometer design based on calculating the measurement uncertainty. The variety in radiometer designs and the demand for improved radiometric measurements justify the need for a more general and comprehensive method to assess system performance. Radiometric resolution, or sensitivity, is a figure of merit that has been commonly used to characterize the performance of a radiometer. However when evaluating the performance of a calibration design for a radiometer, the use of radiometric resolution has limited application. These limitations are overcome by considering instead the measurement uncertainty. A method for calculating measurement uncertainty for a generic radiometer design including its calibration algorithm is presented. The result is a generalized technique by which system calibration architectures and design parameters can be studied to optimize instrument performance for given requirements and constraints. Example applications demonstrate the utility of using measurement uncertainty as a figure of merit.

*Index Terms* – Microwave radiometer calibration, radiometer design, measurement uncertainty analysis, least squares regression.

## 1. Introduction

Radiometer calibration is becoming more important as radiometric measurements are being used to derive greater geophysical information. New applications for microwave and millimeter-wave radiometer data are driving the need for improved radiometric resolution and correspondingly improved accuracy. Finer resolution permits enhanced discrimination of changes in physical parameters from background noise. Accuracy is important for comparing temporal and spatial measurements made from one or many sensors and for using measurements to retrieve parameters by inversion of physical models. Examples of parameters requiring improved resolution and accuracy include the retrieval of sea surface salinity, precipitable water vapor, liquid and ice water path, and vector wind measurements. For a discussion on the principles of radiometry see *Ulaby et al.* [1981], *Kraus* [1966], and *Rohlfs* [1996].

At the core of all radiometers is a calibrated receiver [*Skou*, 1989]. A radiometer receiver is shown in Fig. 1a. Noise power with equivalent brightness temperature $T_{sys}$ enters the receiver and is converted to the output signal v. (In this paper we assume the Raleigh-Jeans limit of the Planck function, and thus, brightness temperature is used as a measure of the band-limited detected power.) The system noise temperature at the receiver input is $T_{sys} = T_{rec} + T_A$, where $T_A$ is the radiant power at the input of the radiometer antenna and $T_{rec}$ is the receiver noise temperature referred to the receiver input. The radiometer response defines the relationship between v and $T_A$; for radiometers utilizing square-law detection, the response is linear and characterized by a slope and offset. The radiometer response fluctuates due to inherent instabilities in the radiometer electronics. *Calibration is the process by which the radiometer response is estimated.* Through calibration an estimate of $T_A$ can be derived from the output signal v. The scheme employed to achieve calibration is central to the design of any radiometer; there exists many techniques for calibrating radiometers.

The advent of the Dicke radiometer in the 1940's spawned radio astronomy and microwave radiometry [*Dicke*, 1946; *Buderi*, 1996]. Since then many improvements in radiometric measurement techniques have developed. Many papers are written on radiometer designs and techniques for analyzing radiometer performance. In recent years the number of publications relating to the analysis of radiometer performance has decreased although the

number of operating radiometer systems and variations in radiometer designs have increased. Advances in RF technology, system control, and numerical processing have greatly expanded the envelop of radiometer capabilities. Today there exists a great number of radiometer designs and nearly as many different implementations of calibration algorithms. Wide variation in calibration designs combined with the need for improved measurements are justification for more general and comprehensive analysis tools for predicting radiometer performance than currently exists.

The primary objective of this paper is to present a generalized technique by which system calibration architectures and design parameters can be studied to optimize instrument performance for a set of given requirements and constraints. A generalized technique for analyzing radiometer designs should provide the means to evaluate the following:

- Tradeoff between time observing the measurand (i.e., the quantity of $T_A$ being measured) and time spent calibrating,
- Effects of interpolating and extrapolating the calibration,
- Influence of calibration reference temperatures on the uncertainty,
- Influence of calibration frequency.

A metric that satisfies these needs is the uncertainty of measurement (or measurement uncertainty). Measurement uncertainty is a parameter that quantifies the dispersion of measured values about the true value of the measurand (i.e., $T_A$) that could reasonably be expected [*ISO*, 1993]. *In this paper, measurement uncertainty is defined as the mean square difference between the estimated value and the true value of the measurand.* Applied to radiometry, measurement uncertainty includes the uncertainty due to the finite radiometric resolution inherent in the measurand observation and uncertainties associated with using imperfect calibration data. Measurement uncertainty as a figure of merit can be applied to the performance of all radiometers.

The American National Standards Institute identifies two approaches for evaluating components of measurement uncertainty [*ANSI*, 1997]. Type A evaluation is based upon statistical analysis of a series of observations. Type B evaluation is based on means other than analysis of observations and usually involves the assumption of a probability distribution function for those factors affecting measurement uncertainty. There is no difference in the nature of uncertainties derived from Type A and Type B analyses; the distinction is made only

to reflect the means by which the uncertainty is evaluated. This paper only addresses measurement uncertainty associated with radiometer designs, and thus, the discussion is limited to Type B analyses.

Measurement uncertainty as a function of calibration frequency depends on the non-stationary stochastic properties of the radiometer pre-detection circuit and receiver electronics. The principles underlying the use of measurement uncertainty as a figure of merit are illustrated by assuming the fluctuations in the radiometer response are wide-sense stationary, i.e., stationary in the first and second moment statistics. Analysis of non-stationary stochastic processes adds a layer of complexity and is not included in this presentation with the exception of brief discussions in Section 3 and Section 7.

A discussion of previous works relevant to radiometer system analysis is presented in Section 2. These works use resolution as a figure of merit for qualifying radiometer performance. Because of its importance to the theme of this paper, the definition of radiometric resolution is examined and the assumptions underlying the classic definition for resolution are reviewed in Section 3 and Appendix A. The limitations in using radiometric resolution to evaluate calibration designs are discussed. In Section 4 a general model for a radiometer design is introduced whereby the calibration architecture is divided into three tiers. A method for evaluating measurement uncertainty based on stochastic signal theory is presented in Section 5. Radiometric resolution is shown to be one component of the measurement uncertainty; other components arise from the estimation of the receiver response. The method presented is applicable to all radiometers with designs that can be decomposed into a set of measurement paths that represent total-power-mode observations. Examples illustrating the application of measurement uncertainty to evaluate different calibration schemes are given in Section 6. A discussion and conclusion follow in Section 7 and Section 8.

## 2. Background

Numerous papers have been written over the past fifty years that have led to improvements in radiometer system performance and analysis. Extensive analysis has been performed on the Dicke radiometer and total power configurations. Contemporary radiometer designs incorporate features of Dicke-type and total-power-mode measurements as well as external measurements to achieve calibration. In some radiometers the recorded output signal

of the system is the difference between signals originating from the measurand and a standard reference. Usually the difference signal is generated by a synchronous detector that performs the subtraction function using analog electronics. Radiometers utilizing this *reference differencing* detection scheme are often referred to as *Dicke radiometers.* In a *switched-reference* detection scheme, observations of the measurand are interleaved with observations of one or more references. Noise injection is a calibration technique where a preset noise power is added into the measurement path. *Reference averaging* is a technique in which multiple observations of a reference are used to improve the resolution of the reference measurement. In *total-power mode* one or more observations of a measurand are made without interleaved observations of a reference.

Reference differencing radiometers have received extensive analysis in the literature [*Tiuri*, 1964; *Wait*, 1967; *Bremer*, 1979; *Thomsen*, 1984]. *Wait* [1967] derives a method using Fourier transforms for analyzing the resolution of reference differencing radiometers. Wait identifies a series of papers that analyze the performance of the reference differencing radiometer but yield differing results for the radiometric resolution. Wait resolves these differences by identifying the divergent assumptions, standardizing the notation, and pointing out errors in published results. A comparison of results is given in a table that contains the radiometric resolution for a number of modulation and correlation waveforms. *Thomsen* [1984] analyzes a reference differencing radiometer with asymmetric switching including the influence of gain fluctuations; however in the limit of symmetric switching (50% duty cycle) with no gain fluctuations, his results differ by $2^{1/2}$ from those of *Kraus* [1966], *Ulaby et al.* [1981], *Wait* [1967], *Bremer* [1979] and others.

*Hach* [1968] presents a measurement technique that utilizes two internal temperature references for calibrating the radiometer. The receiver uses a synchronous detector that periodically switches between the measurand and the two temperature references; the radiometer output is a weighted combination of the three sources. The advantage of this technique over the reference differencing radiometer is that the receiver response, i.e. both slope and offset, is measured every cycle. Hach's design which divides the cycle period between the measurand and the two calibration references suffers a loss of resolution compared to a Dicke-type radiometer. Due to advantages of digital electronics, analog synchronous

detectors rarely appear in new radiometer designs. Rather, it has become more common to numerically process recorded values from individual reference and measurand observations.

The resolution of a reference-differencing radiometer may be improved by a technique presented by *Bremer* [1979]. Bremer demonstrates that significant improvement in performance can be achieved when the reference measurements are averaged over many cycles. Performance is optimized by increasing the portion of the duty cycle that is spent viewing the measurand and increasing the number of reference measurements averaged to reduce the statistical uncertainty in the estimation of the reference value. The improvement in resolution may approach that of a total-power-mode measurement made over the same period. Reference averaging offers significant advantage over the traditional reference-differencing techniques and with the improvements in digital processing the implementation of reference averaging is greatly simplified. Today, reference averaging is commonly used in processing radiometer data.

*Hersman and Poe* [1981] analyze the performance of the total-power mode improving upon previous analysis by including the effects of receiver gain fluctuation and calibration algorithm. In their presentation, radiometric resolution is used as the figure of merit and is defined to be proportional to the integral of the product of the receiver post-detection transfer function and the power spectrum of the square-law detector output (see Appendix A, (A12)). The resulting model accounts for system noise temperature, non-uniform power spectral densities, and processing algorithm parameters such as the calibration period and integration times. Although a formula is presented for a two-point calibration (see equation (9) in *Hersman and Poe* [1981]), the approach fails to account for non-uniform noise components due to the receiver switching between sources. This shortcoming is avoided by assuming the measurand and calibration references have the same noise temperature. An upper limit on the resolution is obtained by setting the observed sources of emission equal to the hottest reference. *Peckham* [1989] extends their work by deriving a set of optimum weights that minimizes the variance of the difference between the weighted average of calibration and measurand samples in the presence of $1/f$-type fluctuations in the receiver. In the limiting case with no gain fluctuations and uniform weighting of the reference measurements the results of *Hersman and Poe* [1981] agree with those presented by *Bremer* [1979].

The references sited above use radiometric resolution as basis for assessing radiometer system performance. Measurement uncertainty is a more appropriate figure of merit for evaluating and comparing radiometer designs. The difference between radiometric resolution and measurement uncertainty is more than semantic. In Section 5 resolution is shown to be one component of the measurement uncertainty and that other components arise from the application of imperfect calibration data. Recognizing the distinction facilitates performance analysis for all types of radiometers. In Section 3 radiometric resolution is defined and evaluated for a simple direct detection radiometer.

## 3. Radiometric Resolution

Radiometric resolution is defined to be the minimum change in the input signal level that can be resolved at the output of the radiometer receiver. Fig. 1b illustrates the relationship between the receiver input noise power and the output signal as a function of time. The radiometer output signal fluctuates because of the inherent stochastic properties of emission and receiver electronics. The mean output signal level, $\bar{v}$, is indicated on the right hand side of the figure and is given by

$$\bar{v}(T_{sys}) = E\{v(t)\}\Big|_{T_{sys}} \tag{1}$$

where the ensemble average includes all possible outputs, $v(t)$, that correspond to the input level $T_{sys}$. A change of signal ($\Delta T$) is considered resolvable at the radiometer output if the ratio of the power in the signal change, $\Delta S_0$, to signal noise power at the output, $N_0$, is equal to or greater than 1 [*Dicke*, 1946; *Kelly et al.*, 1963; *Wait*, 1967,], i.e.,

$$\frac{\Delta S_0}{N_0} \geq 1 \tag{2}$$

The signal noise power is proportional to the variance of the output signal evaluated at the receiver input noise temperature, $T_{sys}$,

$$N_0 \propto \sigma_v^2\Big|_{T_{sys}} = E\{v(t)v(t)\}\Big|_{T_{sys}} - E^2\{v(t)\}\Big|_{T_{sys}} \tag{3}$$

The power in the change of signal is found by truncating the Taylor series expansion of $\overline{v}(T_{sys})$ at the second term for small $\Delta T$, i.e.,

$$\overline{v}(T_{sys}+\Delta T)=\overline{v}(T_{sys})+\Delta T\cdot\frac{\partial\overline{v}}{\partial T}\Big|_{T_{sys}} \quad . \tag{4}$$

For a receiver with a square law detector, the relationship between $\overline{v}$ and $T_{sys}$ is linear; thus, all the change in signal power is contained in the second term of the expansion. The power in the change of the output signal is

$$\Delta S_0 \propto \left(\overline{v}\left(T_{sys}\right)-\overline{v}\left(T_{sys}+\Delta T\right)\right)^2=\left(\Delta T\cdot\frac{\partial\overline{v}}{\partial T}\Big|_{T_{sys}}\right)^2 . \tag{5}$$

Substituting (3) and (5) into (2), noting that the proportionality constant is the same, and solving for $(\Delta T)^2$ yields the classic formula

$$(\Delta T)^2=\frac{\sigma_v^{\,2}}{\left(\frac{\partial\overline{v}}{\partial T}\right)^2}\Big|_{T_{sys}} \quad . \tag{6}$$

The minimum detectable change in signal at the input is equal to the noise power at the output times the reciprocal of the squared response of the system evaluated at $T_{sys}$. Sometimes radiometric resolution is referred to as the noise equivalent temperature difference, i.e. NE$\Delta$T, or sensitivity. Peculiar to microwave engineering, *sensitivity* is synonymous to *resolution.* However in other engineering disciplines, *sensitivity* is more commonly used to describe the change of a system output per change in input stimulus (or its reciprocal) [*ISO*, 1993; *IEEE*, 1996, *Van Putten*, 1996]. The square root of the denominator in (6) is then the radiometer sensitivity. To be more consistent with the engineering community at large, *resolution*, or more specifically *radiometric resolution*, is preferred over *sensitivity* to describe (6).

Fig. 2 shows a model of a direct detection radiometer operating in total-power mode. Noise power $T_A$ enters the radiometer through an antenna. The radiometer receiver is comprised of an amplifier (g), predetection filter (H), square law detector, and a post-detection filter (W). The system noise temperature at the receiver input is $T_{sys}=T_A+T_{rec}$. The radiometer output is the voltage $v(t)$. Evaluating (6) for this radiometer model leads to the classic definition of radiometric resolution [*Dicke*, 1946; *Rohlfs*, 1996]

$$\Delta T\cong\frac{T_{sys}}{\sqrt{B\tau}}$$

(7)

where $B$ is the bandwidth of the predetection filter and $\tau$ is the post-detection integration time constant. These terms are defined by *Tiuri* [1964] and are given in Appendix A. *Rohlfs* [1996] presents a derivation of (7) based upon stochastic signal theory. *Le Vine* [1990] presents a derivation of the resolution for a correlation receiver in an interferometer and shows how the result yields (7) in the limiting case of zero displacement in the antenna elements. In Appendix A, the radiometric resolution of a direct-detection radiometer receiver with gain fluctuations is evaluated. The amplifier gain, $g(t)$, is modeled as a wide-sense-stationary random process with mean $g_0$. For a receiver with gain fluctuations, (6) leads to

$$\Delta T \cong T_{sys} \cdot \left( \frac{1}{B\tau} + \left( \frac{\Delta G}{G} \right)^2 \right)^{1/2} \tag{8}$$

where

$$\left( \frac{\Delta G}{G} \right)^2 = \left( \frac{2}{W(0) \cdot g_0} \right)^2 \int df S_{\tilde{g}}(f) |W(f)|^2 ,$$

and where $S_{\tilde{g}}(f)$ is the power spectrum of the fluctuating component of $g(t)$ and $W(f)$ is the frequency response of the post-detection filter.

Essential to the derivation of (8) is the assumption that $g(t)$ is wide sense stationary. Some authors, [*Kunzi and Magun*, 1977; *Hersman and Poe*, 1981; *Thomsen*, 1984; *Peckham*, 1989], use

$$S_{\tilde{g}}(f) \propto 1/f^{\gamma}$$

to evaluate (8), even though such a spectrum violates the Weiner-Khinchin theorem for $\gamma \geq 1$ [*Davis et al.*, 1996]. One might argue that over a certain interval the gain fluctuations may be considered stationary and, hence, the Fourier relationship between the autocorrelation function and power spectrum exists. In evaluating the influence of calibration frequency on measurement uncertainty, the interval of interest is on the same time scale that the fluctuations in the receiver become non-stationary. The assumption that the stochastic properties of the receiver are stationary may not be justified when studying the interaction between calibration frequency and receiver fluctuations. For this reason, the degree of stationarity [*Huang et al.*, 1998] should be considered when evaluating temporal factors in the calibration algorithm.

The effect of switching between calibration references on radiometric resolution of periodically calibrated radiometers has been investigated [*Bremer*, 1979; *Hersman and Poe*, 1981]. Inevitably, calibration involves observations of references of different brightness temperatures. Evaluation of the output noise power when the input signal power changes when viewing different sources is non-trivial. Difficulty arises in computing the square-law detector output and its convolution with the post-detection transfer function of the radiometer. Furthermore, (6) is evaluated at the system noise temperature. When a radiometer observes sources with different noise temperatures to achieve calibration, $T_{sys}$ necessarily changes. Thus, evaluating (6) in the context of a calibration algorithm is inconsistent with its definition. In the literature these complexities have been avoided by assuming the temperature of the measurand and calibration references are equal thus limiting the usefulness of radiometric resolution as a figure of merit for the performance of a radiometer.

An alternative approach is to consider the measurement uncertainty that includes the resolution of the measurand observation as well as uncertainty associated with applying the calibration data. Before developing a method for evaluating measurement uncertainty, in the following section a general model is introduced that describes a wide variety of calibration architectures.

## 4. General Radiometer Calibration Model

The calibration architecture of most microwave radiometers can be divided into three tiers as illustrated in Fig. 3. Measurements from one or more of the three tiers are used to calibrate the radiometer response. A data processor controls the timing of the calibration reference observation sequence as well as records pertinent data for utilizing the references. In some systems data may be processed in real time to produce estimates of the antenna brightness temperature and others rely on post-processing of the data to calculate the estimates.

First tier calibration consists of calibration references that are switched into the receiver path after the antenna. Calibration structures that fit into this first category include temperature controlled waveguide terminations switched into the receiver path using waveguide switches and active noise sources injected using directional couplers. The first tier is most often used to compensate for fluctuations in the active components of a receiver. Though one or more internal references can be used to track fluctuations in the receiver response, the internal

references do not measure fluctuations that occur in circuitry beyond the plane of the reference measurement, e.g. antenna losses. Usually the equivalent antenna brightness temperature of the references have to be determined through either second or third tier calibration. First tier calibration is utilized when second or third tier calibrations cannot be performed sufficiently rapidly to track receiver fluctuations. Descriptions of radiometers that use first tier calibration can be found in [*Hach*, 1968; *Conglong et al.*, 1986; *Ruf et al.*, 1995; *Racette et al.*, 1998; *Tanner and Riley*, 2003].

The second tier comprises calibration structures that provide a means of calibrating the system response including the effects of the antenna and coupling components. Typically the antenna pattern is projected onto one or more isothermal blackbody radiators. In systems that utilize a second tier structure, characterizing system response is straightforward and can yield accurate calibration since the entire signal path including lossy antenna components is included in the calibration. Several factors limit the practicality of implementing second tier architectures. Blackbody radiators that can envelop the antenna aperture are large, massive, expensive, and prone to errors caused by thermal gradients. Usually a mechanism is needed to switch the field of view of the antenna from the measurand to the calibration reference(s) thus complicating the design of the instrument. Such switching mechanisms are typically slow and contribute to the measurement uncertainty. The Millimeter-Wave Imaging Radiometer [*Racette et al.*, 1996], MARSS [*McGrath and Hewison*, 2001], and the Advanced Microwave Sounding Unit-B (AMSU-B) [*Saunders et al.*, 1995] are examples of radiometers that utilize second tier calibration. The Polarimetric Scanning Radiometer utilizes both first and second tier calibration structures in its calibration scheme [*Corbella et al.*, 2002]. In some radiometer designs the distinction between tier 1 and tier 2 architectures is not clearly delineated. For example, in the TRMM Microwave Imager, a blackbody radiator and cold-space mirror are moved between the primary antenna reflector and the feedhorns [*Wentz et al.*, 2001].

Although second tier calibration provides a means of estimating the system response that includes the effects of antenna losses and coupling mechanisms, additional parameters may be necessary to correct for instrument specific effects such as cross coupling of the calibration references [*Racette et al.*, 1995]. Third tier calibration utilizes measurements external to the instrument. These measurements can then be used to estimate parameters used in the instrument calibration. External references can be blackbody radiators or environmental

sources of emission with known properties. Examples of environmental references include: cosmic radiation, tip-curve calibration, and ocean surface. The third tier often provides the most accurate reference for calibration because the measurements encompass entire system effects and external references, e.g. cosmic radiation, can be as close to an absolute standard that exists. External calibration can also correct for instrument effects that are not measured in first or second tier calibrations. Nevertheless, third tier calibration usually comes with difficulties associated with making the measurement. External reference measurements usually cannot be performed with frequency adequate to track fluctuations in the receiver response. Because of its ability to accurately and precisely characterize entire system effects, third tier calibration is often used to tweak parameters, e.g. antenna coupling losses, effective noise source temperature, etc., in the system equations that describe the radiometer response. An example of the application of third tier architecture applied to calibrating a radiometer is given by *Ruf* [2000]. Ruf describes a technique whereby the properties of the ocean surface brightness temperature are used to correct for a drift in the isolation of a ferrite switch in the TOPEX/Microwave Radiometer.

The Microwave Water Vapor Radiometer (MWR) used by the Department of Energy's Atmospheric Radiation Measurement program is an example of a radiometer that operationally utilizes all three tiers to achieve calibration [*Liljegren*, 2000]. A noise source is injected into the receiver path using a directional coupler. A rotating mirror projects the antenna pattern at an internal blackbody and over a range of elevation angles across the sky. The relation between atmospheric opacity and elevation angle, i.e. tip-curve calibration [*Han and Westwater*, 2000], is used to track the effective noise source temperate and system losses.

It is usual to include parameters in the radiometer calibration to correct for non-idealities in the instrument, e.g. insertion loss, reflections, coupling. Many papers have been written on radiometer system models, parameters to include in the calibration, and techniques for estimating calibration parameters. A technique to correct for coupling between calibration references and the measurand is given by *Racette et al.* [1995]. A technique for transferring internal calibration measurements (tier 1) to an equivalent antenna brightness temperature is given by *Corbella et al.* [2002]. Insertion loss and mismatch effects on radiometric measurements are discussed in [*Hach*, 1968; *Ulaby et al.*, 1981; *Ruf et al.*, 1995; *Stelzried*, 1968; *Miller et al.*, 1967]. Parameters used for calibration are specific to the system design;

values of the parameters and their corresponding uncertainties are specific to the hardware used in the design implementation.

In the following section the uncertainty in the calibrated estimate of the measurand, i.e. measurement uncertainty, is derived. The measurement uncertainty is a function of the individual uncertainties of all the values that go into calculating an estimate of the measurand. The technique can be applied to systems utilizing calibration measurements from one or a combination of tier 1, 2 or 3 architectures.

## 5. Calculation Of Measurement Uncertainty

In this section a technique is presented for evaluating the measurement uncertainty for a radiometer design. First, the design is decomposed into a set of measurement paths. Each measurement path represents a total-power-mode observation and the path's output signal is treated as a separate random process. The radiometer output is then considered as a sequence of samples obtained from the different random processes. The estimate of the measurand is calculated from samples of these random processes. The measurement uncertainty is computed from the statistics of the samples and the functional form of the estimator. To illustrate the technique, a radiometer design based on tier-2 calibration is treated because it is the most simple of cases. To account for differences in signal paths that might exist between calibration measurements, e.g. differences in insertion loss or noise injection modes, is a straight forward extension of the technique. The technique can be applied to all radiometers with designs that can be decomposed into measurement paths that represent total-power-mode observations.

### 5.1. Model Decomposition and Measurement Estimator

Fig. 4a shows a model of a radiometer system that uses tier-2 architecture with a switch to view one of N radiation sources. A radiation source may either be the measurand or one of a number of calibration references. The radiometer output depends on the switch position. At any instance in time the switch is set to only one of its possible N+1 positions; the timing of the switch position sequence is prescribed by $\mathrm{p}(t)$ where $\mathrm{p} \in \{A,1,\ldots,\mathrm{N}\}$. Observations of the measurand correspond to switch position $\mathrm{p} = A$. Fig. 4b illustrates a representation of the system as a set of signal paths, one for each possible value of p. The output of each signal path

is represented by a separate random process. The processes are treated as though each simultaneously exists. Fig. 4c shows a time series of the N+1 processes. The output of the radiometer is a sample of only one of the processes at any given time. By decomposing the radiometer design in this way, transient effects between samples are neglected. Fig. 4d shows a time series of the system output for a particular switch sequence. This presentation is simplified by assuming each process is generated by the same receiver characteristics.

The voltage output of a radiometer operating in total-power mode is given by (A6) in Appendix A. Although the switch position is not explicitly shown, its effect is implicit in the value of $T_{sys}$. For any p, the input to the receiver, $x(t,\mathrm{p})$, is defined to be a zero-mean wide-sense-stationary Gaussian random process with a white power spectrum given by

$$S_x(f,\mathrm{p}) = kT_{sys}(\mathrm{p}) = k\left(T_{rec} + T_{\mathrm{p}}\right) \tag{9}$$

where $k$ is Boltzmann's constant, $T_{rec}$ is the receiver noise temperature referred to the receiver input, and $T_{\mathrm{p}}$ is the antenna brightness temperature for the switch position designated by p. The expected value of the output voltage is a function of the brightness temperature present at the antenna. Evaluating the expected value of (A6) for any given value of p yields

$$E\{\mathrm{v}(t)\}\Big|_{\mathrm{p}} = \bar{\mathrm{v}}(\mathrm{p}) = ckW(0)\cdot\left(T_{rec} + T_{\mathrm{p}}\right)\cdot\left(\int df\,|H(f)|^2\right)\cdot\left(g_0^2 + R_{\tilde{g}}(0)\right) \tag{10}$$

where in Appendix A the symbols are defined and the underlying assumptions are discussed. The ensemble average includes all possible output voltages that correspond to the switch position p. Equation (10) shows the linear relationship between the input brightness temperature to the output voltage. This linear relationship arises from the square-law detection of the input signal. Equation (10) can be rewritten to explicitly show the linear relationship,

$$\bar{\mathrm{v}}_{\mathrm{p}} = \mu T_{\mathrm{p}} + \beta \tag{11}$$

where

$$\mu = ckW(0)\left(\int df\,|H(f)|^2\right)\cdot\left(g_0^2 + R_{\tilde{g}}(0)\right) \tag{12}$$

and

$$\beta = \mu T_{rec}. \tag{13}$$

When sampling the radiometer output, it is not possible to measure the mean value of voltage output given by (10) with zero uncertainty. Thus, the radiometer output is rewritten as the sum of the mean, $\bar{\mathrm{v}}_{\mathrm{p}}$, and a fluctuating component $\tilde{\mathrm{v}}$,

$$\mathrm{v}(t,\mathrm{p}) = \overline{\mathrm{v}}_\mathrm{p} + \tilde{\mathrm{v}}(t,\mathrm{p}) = \mu T_\mathrm{p} + \beta + \tilde{\mathrm{v}}(t,\mathrm{p}) \tag{14}$$

where $\tilde{\mathrm{v}}(t,\mathrm{p})$ is a zero mean random process. The variance of $\tilde{\mathrm{v}}(t,\mathrm{p})$ can be found by evaluating the variance of the output $\mathrm{v}(t,\mathrm{p})$ since $\sigma^2_{\mathrm{v_p}} = \sigma^2_{\tilde{\mathrm{v}}_\mathrm{p}}$. Equation (14) can be rewritten to express the brightness temperature as the dependent variable and the output $\mathrm{v}(t,\mathrm{p})$ as the independent variable, i.e.,

$$T_p = m\mathrm{v}(t,\mathrm{p}) + b + \varepsilon(t,\mathrm{p}) \tag{15}$$

where $m = \mu^{-1}$, $b = -\beta\mu^{-1} = T_{rec}$, and $\varepsilon(t,\mathrm{p}) = -\tilde{\mathrm{v}}(t,\mathrm{p})\mu^{-1}$. The slope $m$ and offset $b$ define the mean system response.

When making measurements with a radiometer, the brightness temperature at the radiometer input is usually not known but is estimated from a measurement of the output voltage. Equation (15) is used as a model to define an estimator for the input brightness temperature. For a *measured* output $\mathrm{v}_\mathrm{p}$, the estimator for the input brightness temperature is

$$\hat{T}_\mathrm{p} = m\mathrm{v}_\mathrm{p} + b\,. \tag{16}$$

The expected value of the estimator is

$$E\{\hat{T}_\mathrm{p}\} = E\{m\mathrm{v}_\mathrm{p} + b\} = m\overline{\mathrm{v}}_\mathrm{p} + b = T_\mathrm{p}\,. \tag{17}$$

The variance of the estimator is

$$\sigma^2_{T_\mathrm{p}} = E\left\{\left(\hat{T}_\mathrm{p} - T_\mathrm{p}\right)^2\right\} = E\{\varepsilon^2_\mathrm{p}\} = \frac{\sigma^2_{\mathrm{v_p}}}{\mu^2}\,. \tag{18}$$

For any given measurement, $\mathrm{v}_\mathrm{p}$, the estimator $\hat{T}_\mathrm{p}$ is a random variable with mean and variance given by (17) and (18), respectively. The fluctuating component $\varepsilon_\mathrm{p}$ arises from the stochastic nature of the signal at the input of the receiver and instabilities within the receiver. This fluctuation is indistinguishable from fluctuations that may exist in $T_\mathrm{p}$. The *standard uncertainty* [*ANSI*, 1997] is the square root of (18). The standard uncertainty in the estimator given by (18) is equal to the radiometric resolution given by (6).

The uncertainty as expressed by (18) is based on the mean system response defined by $m$ and $b$. Generally, $m$ and $b$ in (16) are not known and must be estimated by calibrating the system. An estimate of the measurand, i.e. the unknown antenna brightness temperature, must be obtained by using an estimate of the system response; therefore, the uncertainty in the

estimated antenna brightness temperature should include the uncertainty in the estimates of $m$ and $b$. In the next section estimates of $m$ and $b$ are derived from a set of calibration measurements.

**5.2. Estimating the System Response**

A set of measurements is obtaincd from thc radiomctcr shown in Fig. 4. The measurement set includes $\{\mathrm{v}_A, \mathrm{v}_1, \ldots \mathrm{v}_n, T_1, \ldots, T_n\}$ and is made up of observations of the calibration references and the measurand. The set of measurements is used with Eq. (15) to form a set of equations,

$$\begin{aligned} T_A &= m\mathrm{v}_A + b + \varepsilon_A \\ T_1 &= m\mathrm{v}_1 + b + \varepsilon_1 \\ &\vdots \\ T_n &= m\mathrm{v}_n + b + \varepsilon_n \end{aligned} \tag{19}$$

As in (15), $m$ and $b$ represent the mean response of the system. The value of the measurand, $T_A$, is not known but must be estimated from the data set. The measured voltage, $\mathrm{v}_\mathrm{A}$, is used to estimate the measurand by

$$\hat{T}_A = \hat{m}\mathrm{v}_A + \hat{b} \tag{20}$$

where $\hat{m}$ and $\hat{b}$ are estimates of the system response. The estimator, $\hat{T}_A$, differs from $\widehat{T}_A$ given by (16); $\hat{T}_A$ is an estimate of the antenna brightness temperature based upon estimates of the system response, whereas, $\widehat{T}_A$ is an estimate of the antenna brightness temperature for a known system response. The value of $\varepsilon_A$ in (19) is not known but its variance, $\sigma^2_{T_A}$, is given by (18); its standard deviation is equal to the radiometric resolution of the measurand observation.

Estimates of $m$ and $b$ are derived from the calibration measurements that comprise the remainder of the data set, i.e., $\{T_i, \mathrm{v}_i\}$ where $i \in \{1 \ldots n\}$. The calibration measurement pairs consist of the recorded output voltage, $\mathrm{v}_i$, and the known reference antenna brightness temperature, $T_i$. The $\varepsilon_i$'s are not part of the data set; like $\varepsilon_A$, the values of $\varepsilon_i$'s are not known but their variance are given by (18). When the "true" value of $T_i$ is not known, uncertainty in the knowledge of $T_i$ can be included in the stochastic model of $\varepsilon_i$. Fig. 5 illustrates the set of

measurements. Note that there can be several measurements made at the same temperature $T_i$. The figure shows that $n$ measurements are made at $N$ different temperatures with $N < n$.

There are a number of different ways to use the data in (19) to derive estimates of the system response. For reasons discussed in Section 7, least squares regression (LSR) has been chosen as the framework to obtain $\hat{m}$ and $\hat{b}$. The estimated system response is found by minimizing the sum of the squared errors, i.e. by minimizing E where

$$\mathrm{E} = \sum_{i=1}^{n} \varepsilon_i^2 = \sum_{i=1}^{n} \left( \mathrm{v}_i \hat{m} + \hat{b} - T_i \right)^2 . \tag{21}$$

Applying LSR to the data set yields [*Draper and Smith*, 1998]

$$\hat{m} = \frac{\sum_{i=1}^{n} (\mathrm{v}_i - \overline{\mathrm{v}}_n) T_i}{\sum_{i=1}^{n} (\mathrm{v}_i - \overline{\mathrm{v}}_n)^2} \tag{22}$$

and

$$\hat{b} = \overline{T}_n - \hat{m} \overline{\mathrm{v}}_n \tag{23}$$

where $\overline{T}_n$ and $\overline{\mathrm{v}}_n$ are the arithmetic averages of the calibration data set given by

$$\overline{T}_n = \frac{1}{n} \sum_{i=1}^{n} T_i \tag{24}$$

and

$$\overline{\mathrm{v}}_n = \frac{1}{n} \sum_{i=1}^{n} \mathrm{v}_i . \tag{25}$$

Equations (22) and (23) are the best estimate of the slope and offset when all the measurements in (19) have an equal level of confidence, i.e. $\varepsilon_i$'s have equal variance. However, when the variance of $\varepsilon_i$'s are not equal (which is usually the case), a better estimate of the slope is obtained using weighted least squares regression. When the $\varepsilon_i$'s in (19) are correlated, generalized least squares regression can be used [*Draper and Smith*, 1998]. So long as $\varepsilon_i$'s and $\varepsilon_A$ have zero mean, $\hat{m}$, $\hat{b}$, and $\hat{T}_A$ are unbiased estimators.

**5.3. Standard Uncertainty in the Calibrated Estimate**

The standard uncertainty in the calibrated estimate (20), i.e. measurement uncertainty, is found from the square root of the mean square difference between the estimate and the true value,

$$\sigma_{\hat{T}_A}^2 = E\left\{\left(\hat{T}_A - T_A\right)^2\right\}. \tag{26}$$

In Appendix B (26) is evaluated and found to be

$$\begin{aligned}\sigma_{\hat{T}_A}^2 = \; & \sigma_{T_A}^2 \\ & + \frac{\sum \sigma_{T_i}^2}{n^2} \\ & + \frac{\left(\mathrm{v}_A - \overline{\mathrm{v}}_n\right)^2 \sum \left(\mathrm{v}_i - \overline{\mathrm{v}}_n\right)^2 \sigma_{T_i}^2}{\left(\sum \left(\mathrm{v}_i - \overline{\mathrm{v}}_n\right)^2\right)^2} \\ & + \frac{2\left(\mathrm{v}_A - \overline{\mathrm{v}}_n\right) \sum \left(\mathrm{v}_i - \overline{\mathrm{v}}_n\right) \sigma_{T_i}^2}{n \cdot \sum \left(\mathrm{v}_i - \overline{\mathrm{v}}_n\right)^2}\end{aligned} \tag{27}$$

where $\sigma_{T_i}^2$ and $\sigma_{T_A}^2$ are found from (18) for each of the measurements. The summations are performed over the $i = 1 \ldots n$ measurements. Equation (27) is derived assuming the uncertainties in the calibration measurements are not necessarily equal. Furthermore, $\varepsilon_i$'s are assumed to be independent or, with equivalent effect, the covariance between samples of the receiver output (see (A13) in Appendix A and the discussion following it) is much smaller than the variance of the samples, i.e., $C_v(\Delta t) \ll C_v(0)$ where $\Delta t$ is the time interval between samples.

In order to express the uncertainty of $\hat{T}_A$ in physical terms meaningful to comparative analysis, the relationship $T_p = m\mathrm{v}_p + b$ is substituted into (27) for $\mathrm{v}_p$. After simplification the uncertainty is

$$\sigma_{\hat{T}_A}^2 = \sigma_{T_A}^2 + \frac{\sum \sigma_{T_i}^2}{n^2} + \frac{\left(T_A - \bar{T}_n\right)^2 \sum \left(T_i - \bar{T}_n\right)^2 \sigma_{T_i}^2}{\left(\sum \left(T_i - \bar{T}_n\right)^2\right)^2} + \frac{2\left(T_A - \bar{T}_n\right) \sum \left(T_i - \bar{T}_n\right) \sigma_{T_i}^2}{n \cdot \sum \left(T_i - \bar{T}_n\right)^2} \tag{28}$$

The first term on the right hand side of (28), $\sigma_{T_A}^2$, is the radiometric resolution of the measurand and is the lower limit of the measurement uncertainty. The next three terms arise from the uncertainty in the estimate of the system response and represent the effects of using imperfect calibration data. Equation (28) expresses the uncertainty of the estimated brightness temperature in terms of the resolution of the measurand observation ($\sigma_{T_A}$), uncertainty in the reference measurements ($\sigma_{T_i}^2$), and temperatures of the calibration references ($T_i$). This equation is basis for making quantitative trade studies of the calibration algorithm for a radiometer design using LSR.

Before showing how (28) can be applied to study a system design, it is illustrative to consider the limiting case where all $\sigma_{T_i}^2$'s are equal. Setting $\sigma_{T_i}^2 = \sigma_{T_A}^2$ and simplifying, (28) becomes

$$\sigma_{\hat{T}_A}^2 = \sigma_{T_A}^2 \left(1 + \frac{1}{n} + \frac{\left(T_A - \bar{T}_n\right)^2}{\sum \left(T_i - \bar{T}_n\right)^2}\right). \tag{29}$$

Several observations can be made with regard to (29). The uncertainty in the calibrated response is minimum when the measurement value $T_A$ is equal to the mean of the calibration temperatures. The uncertainty is improved by increasing the separation of the calibration temperatures; the larger separation yields a larger value in the denominator of the third term on the right hand side. The uncertainty is unbounded when all the reference measurements are made at the same reference temperature, i.e. when $T_i = \bar{T}_n$ for $i = 1 \ldots n$. Finally, the uncertainty is improved by increasing the number of calibration measurements. In the limit for increasing $n$, the uncertainty in the calibrated estimate converges to the radiometric resolution.

Least squares regression provides a framework for calculating the measurement uncertainty by which the performance of a calibration design can be assessed. Application of the method is simple and straightforward. In the following section, examples illustrate how LSR can be used to study system design and evaluate the influence of design parameters on instrument performance.

## 6. Application of the Theory

When designing a radiometer there are several constraints applied to the design based upon sampling requirements, operating environments, and limitations due to budgetary or more simply technical difficulties. Even with these constraints there usually exist many degrees of freedom in designing the calibration scheme for the system.

### 6.1. Imaging Radiometer

First consider a design based upon the Millimeter-Wave Imaging Radiometer (MIR). A detailed description of the MIR can be found in [*Racette et al.*, 1996] and a description of the salient characteristics follows. The MIR has five receivers spanning 89 GHz to 340 GHz. The lack of electronic switches at these high frequencies and the short integration times required for imaging led to the decision of using total-power mode. Calibration is achieved by periodically observing two blackbody references at different temperatures. The instrument is designed to fly aboard the NASA ER-2 high-altitude aircraft but has also been used for ground-based atmospheric measurements as well as laboratory studies [*Racette and Wang*, 1998].

Images are generated by a rotating the antenna patterns across a field of view using a flat mirror canted at 45° angle. The across-track swath width is 100° centered about nadir. At cruising altitude of ~20km the ER-2 airspeed is about 200m/s. The nominal full-width half-power beam width for each of the receivers is 3.5°. To achieve contiguous images at half altitude (~10km) the instrument must scan the field of view every 3 seconds. The desire to avoid gaps in the images and the need for frequent calibration to circumvent errors in calibration due to drifts in the receiver gain and offset led to the decision to include calibration observations during each scan cycle. The constraint on the scan cycle period leads to a trade off between time available to observe the measurand and time available to observe the calibration references. A latency interval exists during which time the mirror must switch between the

calibration references and the beginning and end of the field of view. The latency interval also includes the settling time required for the mirror motion and post-detection filters. For the MIR, the latency interval is dominated by the rotation of the scan mirror. However for a system utilizing electronic switches, the time to switch between calibration references and the measurand can be significantly shorter than the settling time of the receiver. Of course it is desirable to keep the latency interval as short as possible.

The total scan period is comprised of three components as follows

$$\tau_{tot} = \tau_s + \tau_{cal} + \tau_{lat} \tag{30}$$

where $\tau_s$ is the time spent observing the measurand, $\tau_{cal}$ is the time spent calibrating, and $\tau_{lat}$ is the latency interval. A relationship between the pixel integration time and calibration integration time can be derived from (30). Assume there are M pixels for each swath scan and that $\tau_s = \mathrm{M}\tau_A$ where $\tau_A$ is the pixel integration time. Furthermore, assume the integration time at each calibration reference is equal to $\tau_i$ and there are N calibration references, $\tau_{cal} = \mathrm{N}\tau_i$. Based upon the requirement for contiguous coverage the cycle period is $\tau_{tot} = 3\,\mathrm{s}$. For the MIR, there are M=56 pixels, N= 2 calibration references, and $\tau_{lat} = 0.5\,\mathrm{s}$. Using these values a relation between the pixel integration time and calibration reference integration time is obtained,

$$\tau_A = \frac{2.5 - 2\tau_i}{56}. \tag{31}$$

Relationship (31) for $\tau_A$ and $\tau_i$ is used in Figs. 6 - 7 to illustrate the tradeoff between integration time and calibration reference temperature. Calculations use pre-detection bandwidth, B = 1 GHz, and the receiver noise temperature $T_{rec} = 500$ K. Regular (unweighted) least squares regression is used in the calculations. (A small improvement results from using weighted LSR.) A single set of calibration measurements, i.e. n = N, are used and gain fluctuations are neglected, i.e. $\tilde{g}(t) = 0$. In the figures that follow, the uncertainty in the measurand brightness temperature estimate is calculated using (28). The uncertainty in the calibration measurements, $\sigma_{T_i}$, and the resolution of the measurand observation, $\sigma_{T_A}$, are calculated from (7) using

$$\sigma_{\mathrm{p}} = \left(T_{rec} + T_{\mathrm{p}}\right)\left(B\tau_{\mathrm{p}}\right)^{-\frac{1}{2}}. \tag{32}$$

advantages of achieving wider temperature separation for the calibration references can be weighed against the additional costs incurred and the performance gained.

### 6.2. Multiple References

Some radiometers use measurements from more than two references to estimate the system response [*Racette et al.*, 1998; *Blackwell et al.*, 2001; *Tanner and Riley*, 2003]. Figure 8 shows how the estimate uncertainty changes with the number of references, i.e. N, used for calibration. Three cases are shown for N=2, N=3, and N=100. The reference temperatures are evenly distributed between $T_c = 250$ K and $T_h = 330$ K, e.g., for N = 3 the reference temperatures are $T_1 = 250$ K, $T_2 = 290$ K, and $T_3 = 330$ K. The calculations assume a fixed time interval for calibration, i.e. $\tau_{cal} = 0.4$ s; the integration times for each reference observation are equal, i.e., $\tau_i = \tau_{cal} N^{-1}$. The latency interval remains fixed, $\tau_{lat} = 0.5\,\mathrm{s}$, independent of the value of N. As in Fig. 6 the pixel integration time is $\tau_A = 38$ ms. The best performance is achieved when only two references are used. A third reference results in marginal deterioration in the estimate uncertainty. The reduced performance can be contrasted with the benefit of having additional degrees of freedom from which goodness of fit can be obtained by the regression. For example, additional reference measurements may be desired to monitor the linearity of the receiver response. Because the uncertainty will increase for larger latency intervals one should anticipate the uncertainty to be worse if adding additional references results in increased latency. The effect is easy to calculate given a model for the latency interval as a function of N.

### 6.3. Reference Averaging

In this section the effect of reference averaging on a calibration scheme is examined. Two cases are considered. In the first case a single reference and measurand observations are interleaved. The results are shown to be consistent with previously published results when the measurand and reference are at the same temperature. In the second case, reference averaging is applied to a calibration scheme which switches between three references and the measurand.

A sequence of measurements is shown in Fig. 9a where observations of the measurand and a single reference are interleaved. The measurand and reference temperatures are $T_A$ and

$T_{ref}$, respectively. The cycle period is $\tau = 1$ second during which time the reference is observed for $\tau_i$ seconds and the measurand is observed for $\tau_A = \tau - \tau_i$. An estimate of the calibration is obtained from $n$ observations of the reference made over an interval $T_W = n\tau$. In order to derive an estimate of the receiver response at least two reference temperatures need to be observed. Hence, a second calibration measurement at temperature, $T_2$, is assumed to occur outside the interval $T_W$; the temperature $T_2$ is different than $T_{ref}$. The uncertainty of this second calibration measurement is assumed to be zero, i.e. $\sigma_{\hat{T}_2} = 0$, in order to minimize its influence on the calculation of measurement uncertainty. In this example, B = 20 MHz and $T_{rec}$ = 500 K are assumed. The uncertainties of the measurand and reference observations are calculated using (32). The measurement uncertainty of a single measurand observation is calculated using (28) and then divided by $\sigma = (T_A + T_{rec}) \cdot (B\tau)^{-0.5}$ to obtain the uncertainty relative to the total-power-mode observation with perfect calibration.

The relative uncertainty for the measurement sequence shown in Fig. 9a is plotted in Fig. 9b. The results shown are for the balanced case where the reference and measurand are the same, i.e. $T_A = T_{rec} = 300$ K. The results do not depend on the temperature of the second calibration reference, $T_2$. For $T_W = 1$ and $\tau_i = 0.5$ s the calculations predict the relative uncertainty is equal to that of a Dicke radiometer with a 50% duty cycle, i.e. two times that of a total-power mode observation of the measurand. The dotted curve in Fig. 9b was calculated using equations (16) and (17) from *Bremer* [1979] which gives the minimum resolution for a balanced ($T_A = T_{ref}$) switched reference radiometer with asymmetric switching. The results of the LSR analysis for the balanced case are consistent with those of Bremer. However for the unbalanced case, i.e. $T_{ref} \neq T_A$, the techniques do not agree; the magnitude and sign of the difference in the techniques depend upon the values used in the calculations. Bremer's formula (see (4) in *Bremer* [1979]) expresses the uncertainty as the root-sum-square of the resolutions of the measurand and reference measurements and does not account for uncertainty in the estimate of the receiver response.

Fig. 10a shows a representative sequence of measurements from a switched-three-reference radiometer. The three reference temperatures are $T_1$ = 300 K, $T_2$ = 500 K and $T_3$ = 800 K. The receiver noise temperature is $T_{rec}$ = 500 K and the pre-detection bandwidth is 20

MHz. The time spent calibrating, $3\tau_i$, is split evenly between the three references; the cycle period is $\tau = 1$ second and the measurand is observed for $\tau_A = \tau - 3\tau_i$; latency due to switching between references is assumed negligible. The measurand brightness temperature is $T_A = 100$ K. The relative uncertainty is calculated the same way as in Fig. 9b.

Fig. 10b illustrates the relationship between the calibration integration time and measurement uncertainty for different observation window lengths, $T_w$, over which reference measurements are used for calibration. The measurement uncertainty has been normalized by the radiometric resolution of a total-power measurement with a 1 second integration time. The curve for $T_W = 1$ s corresponds to a single set of calibration measurements, $n = N = 3$, and yields a minimum uncertainty of ~4.7 times that of the resolution in total-power mode. In this case the measurand is viewed only ~21% of the cycle period. The dashed line indicates the minimum uncertainty as a function of calibration integration time and observation window. Dramatic improvement in measurement uncertainty results by increasing the window over which multiple calibration measurements can be used. Improvement in measurement uncertainty results partly from the increased fraction of time spent observing the measurand and to a greater extent from improving the estimate of the system response. For a 10 minute window, $T_W = 600$ s, the minimum relative uncertainty is 1.16 . When considering large observation windows one should be concerned with the non-stationary fluctuations in the receiver. Calculations using a non-stationary model for the receiver fluctuations (not shown in this paper) reveal that the shapes of the curves in Fig. 10b are largely unaffected, however, for long averaging intervals the curves are shifted upward yielding greater measurement uncertainty.

## 7. Discussion

In the preceding sections, a technique is described whereby measurement uncertainty is used as a figure of merit to assess the performance of a wide-range of radiometer designs. Least squares regression is used as the framework for calibrating the radiometer response and calculating the measurement uncertainty. The LSR approach offers a number of advantages. LSR minimizes the measurement error in the least squares sense and can be applied to a wide variety of calibration designs for performing tradeoff studies of design parameters. LSR provides a simple and straightforward way of computing the measurement uncertainty in terms

of parameters (e.g. standard uncertainty of the calibration measurements) convenient for interpretation; the linear algebra required to compute the measurement uncertainty is easily programmed.

The influence of applying weights to the calibration measurements can be evaluated using weighted LSR. For calibration measurements characterized by Gaussian statistics, the optimum weights are inversely proportional to the standard uncertainty of the calibration measurements. When the calibration measurements are correlated, generalized LSR can be used to include the influence of their correlation.

Methods other than LSR are often used to calibrate the radiometer response and many calibration implementations are not readily expressed as a set of equations in the form of (19). In these cases, the measurement estimate can be expressed as a function of variables that affect the estimate, i.e.

$$\hat{T}_A = f(X_1, X_2, \ldots, X_K) \tag{33}$$

where $X_i$ is the value of the variable, $x_i$. A wide variety of variables may be used in the calculation of the measurement estimate, e.g. reference temperature, insertion loss, reflection coefficient, physical temperature of receiver components, etc. The quantities that contribute to the measurement uncertainty are obtained from random variables whose probability distribution functions model the anticipated fluctuations. The measurement uncertainty is obtained by the law of propagation of uncertainty [*ANSI*, 1997]. For the case where all the variables are independent, the measurement uncertainty is

$$\sigma_{\hat{T}_A}^2 = \sum_{i=1}^{K} \left( \frac{\partial f}{\partial x_i} \right)^2 \sigma_{x_i}^2 \tag{34}$$

where $\sigma_{x_i}^2$ is the variance of $x_i$. It should be noted that the result obtained for the LSR framework, i.e. (27), is a special case of (33) and (34). *Randa* [1998] provides an example application of the law of propagation of uncertainty by calculating the uncertainty in noise-temperature measurements of noise source standards. A comprehensive discussion and treatment of measurement uncertainty including the case for correlated variables is given by [*ANSI*, 1997].

When modeling the measurement uncertainty for a design study, one has freedom in assigning the value of uncertainty to each component of uncertainty. For example if in a design

analysis a noise source exhibits thermal instability, the uncertainty associated with the noise source measurement can be adjusted and its influence on the measurement uncertainty understood. One can then choose to modify the calibration design to compensate for anticipated noise source instability. Thus, type-B analysis of measurement uncertainty can be a valuable aide in understanding the influence of component characteristics on system performance.

Periodic calibration is required to correct for non-stationary fluctuations in the receiver response, e.g. drifts in receiver gain. In this presentation temporal effects such as time interval between calibrations are not considered. This omission is not a limitation of the approach presented. Generally, the uncertainty in the calibration measurement will increase as the interval between the time a calibration measurement is made and the time onto which it is applied increases. The amount by which the uncertainty grows is a function of the non-stationary stochastic properties of the receiver response. The influence of non-stationary fluctuations in the receiver can be assessed by treating the set (or subset) of random processes from which the radiometer output is sampled as non-stationary. The technique outlined in this paper provides a powerful means for studying the nature of non-stationarity in radiometer systems.

## 8. Conclusion

Previously radiometric resolution has been used as a figure of merit to assess the performance of radiometer designs. Radiometric resolution is an important parameter to consider when designing a radiometer, however, difficulties arise when using resolution to evaluate the performance of a calibration design. The evaluation of the ensemble averages required to find the variance of the output signal is complicated by the switching of the input signal between multiple sources. Radiometric resolution is defined and evaluated for a single system temperature ($T_{sys}$), thus, the theoretical basis for using radiometric resolution to characterize the performance of a calibration design is questionable since calibration inevitably involves changing the system temperature. Measurement uncertainty is a more appropriate figure of merit for assessing the performance of a radiometer and its calibration. Measurement uncertainty includes the radiometric resolution of the measurand observation as well as the uncertainty associated with utilizing the calibration data.

A general radiometer calibration model is introduced that describes a wide variety of calibration architectures. Most radiometers contain calibration features from one or more of the three tiers identified by the model. Regardless from which tier an observation is made, the observed signal can be modeled by a random process; all signals observed are treated as originating from simultaneously existing random processes. The radiometer output is thus comprised as a sequence of samples obtained from a set of different random processes. The statistics of the calibration reference and measurand samples are derived from the properties of the underlying random processes. The statistics are then used with the functional form of the calibration algorithm to compute the measurement uncertainty. The technique presented can be applied to all radiometer designs that can be decomposed into a set of measurement paths that represent total-power-mode observations.

LSR is used as a framework for modeling the calibration algorithm although the theoretical basis for using measurement uncertainty to assess the performance of radiometer designs extends to a broader range of calibration algorithms. The utility of measurement uncertainty as a figure of merit is demonstrated by evaluating the influence of calibration reference temperatures, number of calibration references, integration time of the calibration references, integration time of the measurand, and reference averaging. The technique presented has been applied to evaluating calibration designs using two and more calibration references and to systems utilizing reference averaging. The effect of interpolating and extrapolating calibration data on measurement uncertainty is shown. The optimum fraction of time spent observing the measurand is shown to depend on the calibration reference temperatures.

This work focused on developing techniques for radiometer design analysis and is limited to type-B uncertainty analysis. For analyzing the measurement uncertainty of actual radiometer systems, the combined uncertainty including type-A and type-B analyses should be considered.

**Acknowledgement.** The authors would like to thank Dr. Ed. Westwater for valuable discussions that contributed to the development of the work presented. The authors would also like to thank Dr. David LeVine and Dr. Jeffrey Piepmeier for insightful comments that lead to improvements in the paper. This work was conducted in support of NASA's Earth Science Enterprise at the Goddard Space Flight Center.

## Appendix A

In this appendix the radiometric resolution is evaluated for a direct detection radiometer with gain fluctuations operating in total-power mode. A model for such a radiometer is shown in Fig. 2 and described in Section 3. The input signal to the radiometer receiver, *x(t)*, is assumed to be a zero-mean Gaussian random process with a white noise power spectrum given by

$$S_x(f) = kT_{sys}. \tag{A1}$$

where $k$ is Boltzman's constant and $T_{sys}$ is the system noise temperature. The impulse responses of the pre-detection and post-detection filters are $h(t)$ and $w(t)$, respectively. The frequency responses of the filters are given by the Fourier transform pairs,

$$W(f) = \int_{-\infty}^{\infty} w(t)e^{-i\omega t}dt \qquad H(f) = \int_{-\infty}^{\infty} h(t)e^{-i\omega t}dt \tag{A2}$$

where $\omega = 2\pi f$. The bandwidth of the pre-detection filter is assumed to be much larger than the bandwidth of the post-detection filter. The amplifier gain is expressed as the sum of the mean and a fluctuating component, i.e.,

$$g(t) = g_0 + \tilde{g}(t) \tag{A3}$$

where $g_0$ is the mean value of $g(t)$ and $\tilde{g}(t)$ is the fluctuating component. The fluctuating component is modeled as a zero-mean Gaussian random process. By assuming $\tilde{g}(t)$ is wide-sense-stationary, the Fourier transform relationship between its autocorrelation function and power spectrum exists, such that

$$E\{\tilde{g}(t_1)\tilde{g}(t_2)\} \equiv R_{\tilde{g}}(\Delta t) = \int_{-\infty}^{\infty} S_{\tilde{g}}(f)e^{i\omega\Delta t}df \tag{A4}$$

where $\Delta t = t_2 - t_1$, and $R_{\tilde{g}}(\Delta t)$ and $S_{\tilde{g}}(f)$ are the autocorrelation and power spectrum of $\tilde{g}(t)$, respectively. In the proceeding analysis, it is assumed that *g(t)* and *x(t)* are independent and that the fluctuation in $\tilde{g}(t)$ is much slower than the impulse response of $h(t)$. The fluctuation can exist on the same time scale as the impulse response of the post-detection filter.

The receiver input passes through an amplifier, filter, and an ideal square-law detector. The output of the square law detector is denoted *y(t)*; and v*(t)* is the voltage output of the post-detection filter. By assuming the gain fluctuations are slow, the output of the amplifier can be expressed as the instantaneous product *x(t)g(t)*. The output of the square law detector is

$$y(t) = c\left(x(t)\,g(t) \otimes h(t)\right)^2 \tag{A5}$$

where $\otimes$ is the convolution operator, $c$ is the gain of the square-law detector (usually expressed in units of Volts per Watts). The output of the post-detection filter is

$$\mathrm{v}(t) = y(t) \otimes w(t). \tag{A6}$$

The resolution is found by evaluating (6). First consider the denominator; using the above stated assumptions it is straightforward to show that

$$\left(\frac{\partial}{\partial T} E\{\mathrm{v}(t)\}\right)^2\Bigg|_{T=T_{sys}} = c^2 W^2(0) k^2 \left(\int_{-\infty}^{\infty} |H(f)|^2\, df\right)^2 \left(g_0^2 + R_{\tilde{g}}(0)\right)^2. \tag{A7}$$

Evaluation of the numerator is more involved since it requires finding the variance of the output which in turn involves evaluating the fourth moment statistics of *g(t)* and *x(t)*. The variance is found from the zero-lag covariance function of the receiver output. The covariance function is given by

$$C_{\mathrm{v}}(\Delta t) = \int_{-\infty}^{\infty} S_y(f) |W(f)|^2 e^{-i\omega\Delta t}\, df - E^2\{\mathrm{v}(t)\}\Big|_{T=T_{sys}} \tag{A8}$$

where $S_y(f)$ is the power spectrum at the output of the square law detector and is found from the Fourier transform of the autocorrelation function

$$R_y(\tau) = E\{y(t)\,y(t+\tau)\}. \tag{A9}$$

Evaluating (A9) requires calculating the forth moment expected averages of *x(t)* and *g(t)*. In this calculation the relationship,

$$E\{x(t_1)x(t_2)x(t_3)x(t_4)\} = R_{x_{12}}R_{x_{34}} + R_{x_{13}}R_{x_{24}} + R_{x_{14}}R_{x_{23}}, \tag{A10}$$

for zero-mean Gaussian random processes is used where $R_{x_{ij}} = E\{x(t_i)x(t_j)\}$. To evaluate (A9), substitute the corresponding Fourier transforms for $R_x(\bullet)$ and $R_{\tilde{g}}(\bullet)$, apply the Fourier

exponents to transform the filter impulse responses to the frequency domain, utilize the assumption that the bandwidth of $H(f)$ is much larger than the bandwidth of $S_{\tilde{g}}(f)$, and term by term use the remaining integrals to transform the power spectrum of the gain fluctuations back into the time domain. After grouping like terms,

$$\begin{aligned} R_y(\Delta t) = c^2 R_H^2(0)\cdot\left[g_0^4 + 2g_0^2 R_{\tilde{g}}(0) + R_{\tilde{g}}^2(0) + 2R_{\tilde{g}}^2(\Delta t) + 4g_0^2 R_{\tilde{g}}(\Delta t)\right] + \\ 2c^2 R_H^2(\Delta t)\cdot\left[g_0^4 + 2g_0^2 R_{\tilde{g}}(0) + R_{\tilde{g}}^2(0) + 2R_{\tilde{g}}^2(\Delta t) + 4g_0^2 R_{\tilde{g}}(\Delta t)\right] \end{aligned} \quad \text{(A11)}$$

where

$$R_H(\Delta t) = \int_{-\infty}^{\infty} S_x(f)\left|H(f)\right|^2 e^{i\omega\Delta t} df .$$

By subtracting the DC component from (A11), (A12) may be expressed as

$$C_v(\Delta t) = \int_{-\infty}^{\infty} S_r(f)\left|W(f)\right|^2 e^{i\omega\Delta t} df \quad \text{(A12)}$$

where

$$\begin{aligned} S_r(f) = 2c^2 R_H^2(0)\left(S_{\tilde{g}} \otimes S_{\tilde{g}}\right) + 4c^2 R_H^2(0) g_0^2 S_{\tilde{g}} + \\ \left(2c^2 g_0^4 + 6c^2 R_{\tilde{g}}^2(0) + 12c^2 g_0^2 R_{\tilde{g}}(0)\right)\cdot S_H \otimes S_H \end{aligned}$$

and $S_H$ is the Fourier transform of $R_H$. The variance of the output is found by evaluating (A12) with $\Delta t = 0$. It is noteworthy to observe that the variance obtained from (A12) is the starting point for analysis presented in *Hersman and Poe*, [1981].

Substituting (A1) into (A12) and making use of the bandwidth assumption between the pre-detection and post-detection filters yields

$$\begin{aligned} C_v(\Delta t) = \left[\left(g_0^4 + 3R_{\tilde{g}}^2(0) + 6g_0^2 R_{\tilde{g}}(0)\right)2c^2 k^2 T_{sys}^2 \int_{-\infty}^{\infty} df' \left|H(f')\right|^4\right] \int_{-\infty}^{\infty} df \left|W(f)\right|^2 e^{i\omega\Delta t} \\ + 4c^2 g_0^2 k^2 T_{sys}^2 \left[\int_{-\infty}^{\infty} df' \left|H(f')\right|^2\right]^2 \int_{-\infty}^{\infty} df'' \left|W(f'')\right|^2 S_{\tilde{g}}(f'') e^{i\omega\Delta t} \end{aligned} \quad \text{(A13)}$$

The first term on the right hand side of (A13) is the covariance due to the band-limited noise at the receiver input; this term gives rise to (7) and its correlation interval is governed by the bandwidth of the post-detection filter. Receiver gain fluctuations give rise to the second term on the right hand side. For gain fluctuations that are slow with respect to $\Delta t$ and small in magnitude compared to $g_0$, the covariance function of the receiver output can be expressed as

$$C_v(\Delta t) = 2g_0^4 c^2 k^2 T_{sys}^2 \int_{-\infty}^{\infty} df' \left|H(f')\right|^4 R_W(\Delta t) + 4c^2 g_0^2 k^2 T_{sys}^2 \left[\int_{-\infty}^{\infty} df' \left|H(f')\right|^2\right]^2 W^2(0) R_{\tilde{g}}(\Delta t) \quad \text{(A14)}$$

where

$$R_W(\Delta t) = \int_{-\infty}^{\infty} df \left|W(f)\right|^2 e^{i\omega\Delta t} \; . \quad \text{(A15)}$$

The covariance function given by (A14) is a linear combination of $R_W$ and $R_{\tilde{g}}$ scaled by $g_0^4$ and $g_0^2$, respectively. The contribution of $R_{\tilde{g}}$ is usually negligible for computing the output variance since receiver gain fluctuations are typically small over the integration interval defined by $W(f)$. The contribution of $R_W$ to the covariance between sequential samples, e.g. calibration observations, is usually very small since $R_W$ tends to decay rapidly on time scales longer than the sampling interval. Gain fluctuations become more predominant for the covariance between samples as the time interval increases. Although we have assumed stationarity, one must keep in mind that gain fluctuations are inherently non-stationary; $R_{\tilde{g}}(\Delta t)$ may not adequately represent the gain fluctuations since it is an autocorrelation function of a wide-sense-stationary process. The covariance function given by (A13) is valid for time intervals over which the fluctuations can be considered stationary. It should be noted that the covariance given by (A13) changes slightly when the time interval encompasses observations at two different system temperatures, i.e. $T_{sys}^2 \rightarrow T1 \cdot T2$ where $T1$ and $T2$ are the system temperatures at the two times.

The radiometric resolution is obtained by substituting (A7) and the variance obtained from (A13) into (6). The following definitions are adopted from *Tiuri*, [1964]. The pre-detection bandwidth is

$$B = \frac{\left(\int_{-\infty}^{\infty} \left|H(f)\right|^2 df\right)^2}{\int_{-\infty}^{\infty} \left|H(f)\right|^4 df} \quad \text{(A16)}$$

and the post-detection integration time constant is

$$\tau = \frac{W^2(0)}{2\int_{-\infty}^{\infty} |W(f)|^2 \, df}. \tag{A17}$$

After making the substitutions

$$\left(\frac{\Delta T}{T_{sys}}\right)^2 = \frac{2\int_{-\infty}^{\infty} \left(S_{\tilde{g}} \otimes S_{\tilde{g}} + 2g_0^2 S_{\tilde{g}}\right)|W(f)|^2 \, df}{\left(g_0^2 + R_{\tilde{g}}(0)\right)^2 W^2(0)} + \left(\frac{g_0^4 + 3R_{\tilde{g}}^2(0) + 6g_0^2 R_{\tilde{g}}(0)}{\left(g_0^2 + R_{\tilde{g}}(0)\right)^2}\right)\frac{1}{B\tau}. \tag{A18}$$

By making the assumption that the mean gain is much larger than the gain fluctuations, i.e. $g_0^2 \gg R_{\tilde{g}}(0)$, (A18) can be further simplified to obtain (8).

It is interesting to see how (A18) relates to other published forms of resolution for receivers with gain fluctuations [*Ulaby et al.*, 1981; *Rohlfs*, 1996]. To do this, assume that the voltage gain is a Gaussian random variable and substitute $S_{\tilde{g}}(f) = \sigma_{\tilde{g}}^2 \delta(f)$ into (A18) where $\delta(f)$ is the Kronecker delta function. Next define the power gain as $G = g^2$. Using the properties of the Gaussian random variable [*Davenport and Root*, 1987], the power gain is also a Gaussian random variable with mean

$$G_0 = E\{G\} = E\{g^2\} = g_0^2 + \sigma_{\tilde{g}}^2 \tag{A19}$$

and variance

$$(\Delta G)^2 = E\left\{(G - G_0)^2\right\} = 2\sigma_{\tilde{g}}^4 + 4g_0^2\sigma_{\tilde{g}}^2. \tag{A20}$$

Upon substituting these definitions into (A18), one obtains

$$\left(\frac{\Delta T}{T_{sys}}\right)^2 = \left(\frac{\Delta G}{G_0}\right)^2 + \frac{1}{B\tau}. \tag{A21}$$

## Appendix B

The uncertainty in $\hat{T}_A$ is found by evaluating the expected value of the square of the difference between the estimated value and actual value, i.e.

$$\sigma_{\hat{T}_A}^2 = E\left\{\left(\hat{T}_A - T_A\right)^2\right\}. \tag{B1}$$

It is convenient to express

$$\hat{T}_A = \left(\mathrm{v}_A - \bar{\mathrm{v}}_\mathrm{n}\right)\hat{m} + \bar{T}_n \tag{B2}$$

where $\hat{b} = \bar{T}_n - \hat{m}\bar{\mathrm{v}}_\mathrm{n}$ has been substituted into (20); and likewise to express

$$T_A = \left(\mathrm{v}_A - \bar{\mathrm{v}}_\mathrm{n}\right)m + \bar{T}_n - \bar{\varepsilon}_n + \varepsilon_A \tag{B3}$$

Equation (B3) is obtained by substituting $b = \bar{T}_n - m\bar{\mathrm{v}}_\mathrm{n} - \bar{\varepsilon}_n$ into $T_A = m\mathrm{v}_A + b + \varepsilon_A$ from (19). The arithmetic means $\bar{T}_n$ and $\bar{\mathrm{v}}_n$ are given by (24) and (25), respectively, and

$$\bar{\varepsilon}_n = \frac{1}{n}\sum_{i=1}^{n}\varepsilon_i \,. \tag{B4}$$

Substituting (B3) and (B2) into (B1) yields

$$\sigma^2_{\hat{T}_A} = E\left\{\varepsilon_A^2\right\} + E\left\{\bar{\varepsilon}_n^2\right\} + \left(\mathrm{v}_A - \bar{\mathrm{v}}_\mathrm{n}\right)^2 E\left\{\left(\hat{m}-m\right)^2\right\} + 2\left(\mathrm{v}_A - \bar{\mathrm{v}}_\mathrm{n}\right)E\left\{\left(\hat{m}-m\right)\bar{\varepsilon}_n\right\}. \tag{B5}$$

In evaluating (B5), the contribution of the gain fluctuations to the correlation between samples, i.e., $R_{\tilde{g}}\left(\Delta t_{ij}\right)$ in (A14) where $\Delta t_{ij}$ is the time between samples, are assumed to be negligibly small. Thus, $\varepsilon_i$'s are treated as independent so that $E\left\{\varepsilon_i\varepsilon_j\right\} = \delta_{ij}\sigma_i^2$ where $\delta_{ij}$ is the Kronecker delta function. One obtains

$$\hat{m} - m = \frac{\sum\left(\mathrm{v}_i - \bar{\mathrm{v}}_\mathrm{n}\right)\varepsilon_i}{\sum\left(\mathrm{v}_i - \bar{\mathrm{v}}_\mathrm{n}\right)^2} \tag{B6}$$

by substituting $T_i = m\mathrm{v}_i + b + \varepsilon_i$ into (22). After substituting (B6) and (B4) into (B5) and evaluating the expected averages, (27) is obtained.

**References**

ANSI, *American National Standard for Calibration – U.S. Guide to the expression of uncertainty in measurement*, ANSI/NCSL Z540-2-1997, 1997.

Blackwell, W.J., J.W. Barrett, F.W. Chen, R.V. Leslie, P.W. Rosenkranz, M.J. Schwartz, and D. H. Staelin, NPOESS Aircraft Sounder Testbed-Microwave (NAST-M): instrument description and initial flight results, *IEEE Trans. Geosci. Rem. Sensing*, 39(11), 2444-2453, 2001.

Bremer, J. Improvement of Scanning Radiometer Performance by Digital Reference Averaging, *IEEE IM*, 28(1), 46 – 54, 1979.

Buderi, R. *The invention that changed the world: how a small group of radar pioneers won the Second World War and launched a technological revolution*, Simon & Schuster, New York, NY, 1996.

Conglong, Z., J.B. Snider, D.C. Hogg, Computer Demodulation Technique for a Dual-Channel Microwave Radiometer, *Advances in Atmospheric Sciences*, 3(2), 189-198, 1986.

Corbella, L, A.J. Gasiewski, M. Klein, V. Leuski, A.J. Francavilla, and J.R. Piepmeier, On-board accurate calibration of dual-channel radiometers using internal and external references, *IEEE Trans. on Microwave Theory and Techniques*, 50(7), 1816 – 1820, 2002.

Davenport, W.B., W. Root, *An Introduction to the Theory of Random Signals and Noise*, reprinted by IEEE Press, New York, NY, 1987. (Originally published by McGraw Hill Book Company, 1958).

Davis, A., A. Marshak, W. Wiscombe, and R. Cahalan, Scale Invariance of Liquid Water Distribution in Marine Stratocummulus, Part 1: Spectral Properties and Stationary Issues, *J. of Atmos. Sci.*, 53(11), 1996.

Dicke, R.H., The measurement of thermal radiation at microwave frequencies, *Rev. Sci. Instr.*, 17, 268 - 279, 1946.

Draper, N. R., H. Smith, *Applied Regression Analysis, Third Edition*, John Wiley and Sons, Inc., New York, 1998.

Hach, J.P., A very Sensitive Airborne Microwave Radiometer Using Two Reference Temperatures, *IEEE Trans. on Microwave Theory and Techniques*, 16(9), 629 – 636, 1968.

Han, Y., E. R. Westwater, Analysis and improvement of tipping calibration for ground-based microwave radiometers, *IEEE Trans. Geosci. Rem. Sensing*, 38(3), 1260-1276, 2000.

Hersman, M.S., G.A. Poe, Sensitivity of the Total Power Radiometer with Periodic Absolute Calibration, *IEEE Trans. on Microwave Theory and Techniques*, 29(1), 32 – 40, 1981.

Huang, N. E., Z. Shen, S. R. Long, M. C. Wu, H. S. Hsing, Q. Zheng, N-C. Yen, C. C. Tung, and H. H. Liu, The emperical mode decomposition and the Hilbert Spectrum for nonlinear and non-stationary time series analysis, *Proceedings of the Royal Society*, 454, 903-995, 1998.

IEEE, *The IEEE Standard Dictionary of Electrical and Electronic Terms*, IEEE Standard 100, 1996.

ISO, *International Vocabulary of Basic and General Terms in Metrology. Second Edition,* International Organization for Standardization, Switzerland, 1993.

Kelly, E.J., D.H. Lyons, and W.L. Root, The Sensitivity of Radiometric Measurements, J. Soc. Indust. Appl. Math., Vol. 11, No. 2, pp. 235 – 257, June, 1963.
Kraus, J.D., *Radio Astronomy*, Cygnus Quasar Books, Powell, OH, 1966.

Kunzi, K., A. Magun, Statistical gain fluctuations of microwave amplifiers measured with a Dicke-radiometer, *Math Phys.*, 22, 404-411, 1977.

Le Vine, D.M., The sensitivity of synthetic aperture radiometers for remote sensing applications from space, *Radio Sci.*, 25(4), 441-453, 1990.

Liljegren, J. C., Automatic Self-Calibration of ARM Microwave Radiometers, in *Microwave Radiometry and Remote Sensing of the Earth's Surface and Atmosphere*, pp. 433-441, edited by P. Pampaloni and S. Paloscia, VSP Press, 2000.

McGrath, A., T. Hewison, Measuring the accuracy of MARSS - An airborne microwave radiometer, *J. Atmos. Oceanic Techn.*, 18(12), 2003-2012, 2001.

Miller, C.K.S., W.C. Daywitt, and M.G. Arthur, Noise standards, measurements, and receiver noise definitions, *Proc. of the IEEE*, 55(6), 865 – 877, 1967.

Papoulis, A., *Probability, Random Variables, and Stochastic Processes*, McGraw-Hill, New York, NY, 1991.

Peckham, G.E., An Optimum calibration procedure for radiometers, *Int. J. Remote Sensing*, 10(1), 227-236, 1989.

Racette, P., R. F. Adler, J. R. Wang, A. J. Gasiweski, D. M. Jackson, and D. S. Zacharias, An airborne millimeter-wave imaging radiometer for cloud, precipitation, and atmospheric water vapor studies, *J. Atmos. Oceanic Techn.*, 13(3), 610 – 619, 1996.

Racette, P., M. Triesky, and D.C. Jones, A multi-channel microwave radiometer uses reference averaging for calibration: precision approaches that of a total power radiometer, Proc. International Geophysics And Remote Sensing Symposium '98, IEEE-GRSS, Seattle, WA July, 1998.

Racette, P., J. R. Wang, Passive millimeter- and sub-millimeter-wave imaging for atmospheric research, Proceedings of the International Society for Optical Engineering 12th Annual Symposium, Orlando, FL, April 1998.

Racette, P., J. R. Wang, P. Evans, R. Saunders, A. Gasiewski, and D. Jackson, A calibration experiment using millimeter-wave imaging radiometer at the UK meteorological office calibration facility, Proc. International Geophysics And Remote Sensing Symposium '98, IEEE-GRSS, Florence, Italy, July 1995.

Randa, J., Uncertainties in NIST Noise Measurements, NIST Technical Note 1502, March 1998.

Rohlfs, K., T.L. Wilson, *Tools of Radio Astronomy*, Springer-Verlag, New York, NY, 1996.

Ruf, C.S., Detection of calibration drifts in spaceborne microwave radiometers using a vicarious cold reference, *IEEE Trans. Geosci. Rem. Sensing*, 38(1), 44 – 52, 2000.

Ruf, C. S., S.J. Keihm, and M.A. Janssen, TOPEX/Poseidon Micorwave Radiometer (TMR): I. Instrument Description and Antenna Temperature Calibration, *IEEE Trans. Geosci. Rem. Sensing*, 33(1), 125 – 137, 1995.

Saunders, R.W., T.J. Hewison, S.J. Stringer, and N.C. Atkinson, The Radiometric Characterization of AMSU-B, *IEEE Trans. on Microwave Theory and Techniques*, 43(4), 760 – 771, 1995.

Skou, N. *Microwave Radiometer Systems: Design and Analysis*, Artech House, Norwood, MA, 1989.

Stelzried, C.T., Microwave thermal noise standards, *IEEE Trans. on Microwave Theory and Techniques*, 16(9), 646 – 655, 1968.

Tanner, A., and A. Lance Riley, Design and performance high-stability water vapor radiometer, *Radio Sci.*, 38(3), 2003.

Thomsen, F. On the Resolution of Dicke-Type Radiometers, *IEEE Trans. on Microwave Theory and Techniques*, 32(2), 145 – 150, 1984.

Tiuri, M.E., Radio Astronomy Receivers, *IEEE Trans. on Mil. Electro.*, 8, 264-272 (1964).

Ulaby, F.T., R.K. Moore, and A.K. Fung, *Microwave Remote Sensing: Active and Passive, Vol I, Microwave Remote Sensing Fundamentals and Radiometry*, Addison Wesley Publishing Company, Reading, MA, 1981.

Van Putten, A.F.P., *Electronic Measurement Systems, Theory and Practice*, pp. 110 – 152, Institute of Physics Publishing, Philadelphia, PA, 1996.

Wait, D.F., The Sensitivity of the Dicke Radiometer, *J. of Research of the National Bureau of Standards*, 71(2), 127 – 152, 1967.

Wentz, F. J., P. Ashcroft, and C. Gentemann, Post-Launch Calibration of the TRMM Microwave Imager, *IEEE Trans. Geosci. Rem. Sensing*, 39(2), 415 – 422, 2001.

**Figure List**

1. (a) Illustration of a basic radiometer model with input brightness temperature $T_{sys}$ and output voltage v. (b) Graph illustrating the principle of measurement resolution.
2. Block diagram of a direct detection radiometer making a total-power mode measurement. The radiometer is comprised of an antenna, amplifier, pre-detection filter, square-law detector and post-detection filter.
3. Generic model for radiometer calibration architecture illustrating three tiers of calibration. Tier 3 comprises calibration references external to the radiometer, e.g. cosmic background radiation, ocean surface. Calibration references that are included as part of the radiometer system and are observed through the antenna are in Tier 2. Calibration references internal to the radiometer receiver and not observed through the antenna are in Tier 1, e.g. noise source injection.
4. (a) A model of a radiometer with a switch used to view one of N + 1 radiation sources. The switch position is controlled by p(t). (b) The radiometer is expanded as a set of subsystems with each subsystem representing a different measurement path. (c) The signals out of the subsystems form a set of simultaneously existing random processes. (d) The radiometer output is a sequence of samples from the set of random processes.
5. Graphical illustration of a calibration data set of $n$ measurements made at N different temperatures with $n > N$. The dashed line is the response of the radiometer.
6. Standard measurement uncertainty versus measurand brightness temperature for two pairs of calibration target temperatures. The circles and x's on the abscissa indicate the temperatures of the calibration references. The dotted curve shows the resolution of the measurand observation.
7. Standard measurement uncertainty as a function of time spent at each calibration reference (bottom abscissa) and time spent observing the measurand (top abscissa) for two pairs of calibration target temperatures. The dotted curve shows the resolution of the measurand observation.
8. Standard measurement uncertainty as a function of measurand temperature for different numbers of reference temperatures used in the calibration. Reference temperatures are evenly distributed between 250 K and 330 K.

9. (a) A diagram of a time series of measurements from a single-reference switched radiometer. Reference-averaging is applied to the reference measurements over an interval $T_W$. A second reference, $T_2$, is observed with zero uncertainty outside the interval $T_W$. (b) The relationship between the reference-averaging window width, the reference integration time, and relative uncertainty is shown for the case when $T_{ref} = T_A = 300$ K. The dotted curve indicates the minimum as predicted by *Bremer* [1979].
10. (a) A diagram of a time series of measurements illustrating a window over which reference-averaging is applied to the calibration measurements. (b) The relationship between the reference-averaging window width, the calibration reference integration time, and relative uncertainty. The dotted curve is the minimum relative uncertainty calculated over a range of $T_W$.

**Figure 1**

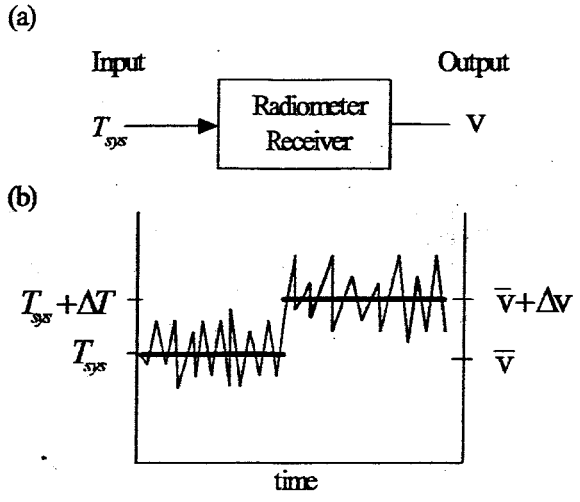


Figure 1: (a) Illustration of a basic radiometer model with input brightness temperature $T_{sys}$ and output voltage v. (b) Graph illustrating the principle of measurement resolution.

**Figure 2**

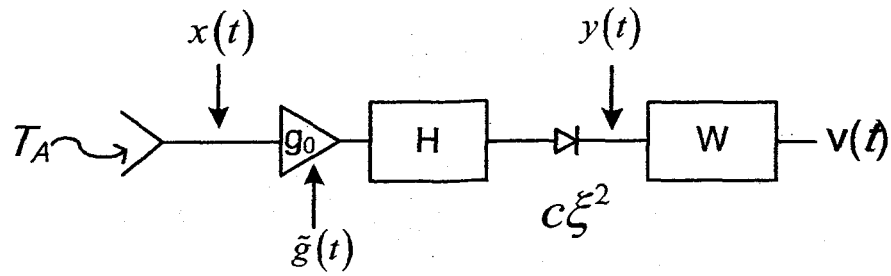


Figure 2: Block diagram of a direct detection radiometer making a total-power mode measurement. The radiometer is comprised of an antenna, amplifier, pre-detection filter, square-law detector and post-detection filter.

**Figure 3**

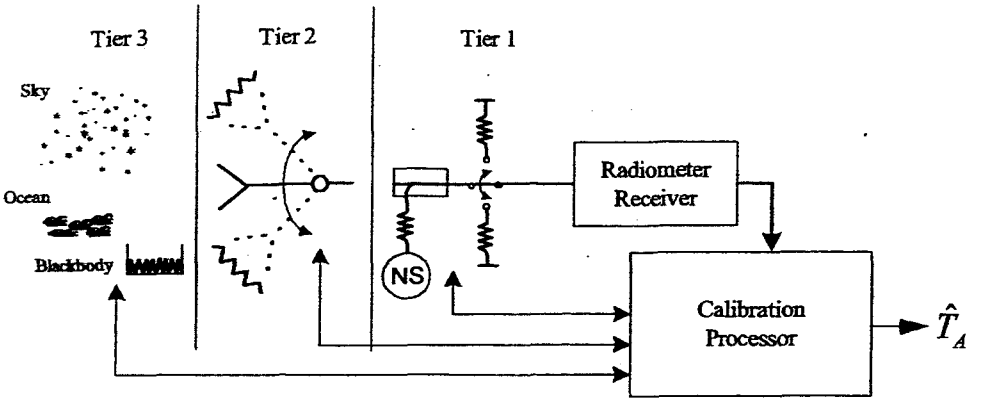


Figure 3: Generic model for radiometer calibration architecture illustrating three tiers of calibration. Tier 3 comprises calibration references external to the radiometer, e.g. cosmic background radiation, ocean surface. Calibration references that are included as part of the radiometer system and are observed through the antenna are in Tier 2. Calibration references internal to the radiometer receiver and not observed through the antenna are in Tier 1, e.g. noise source injection.

**Figure 4**

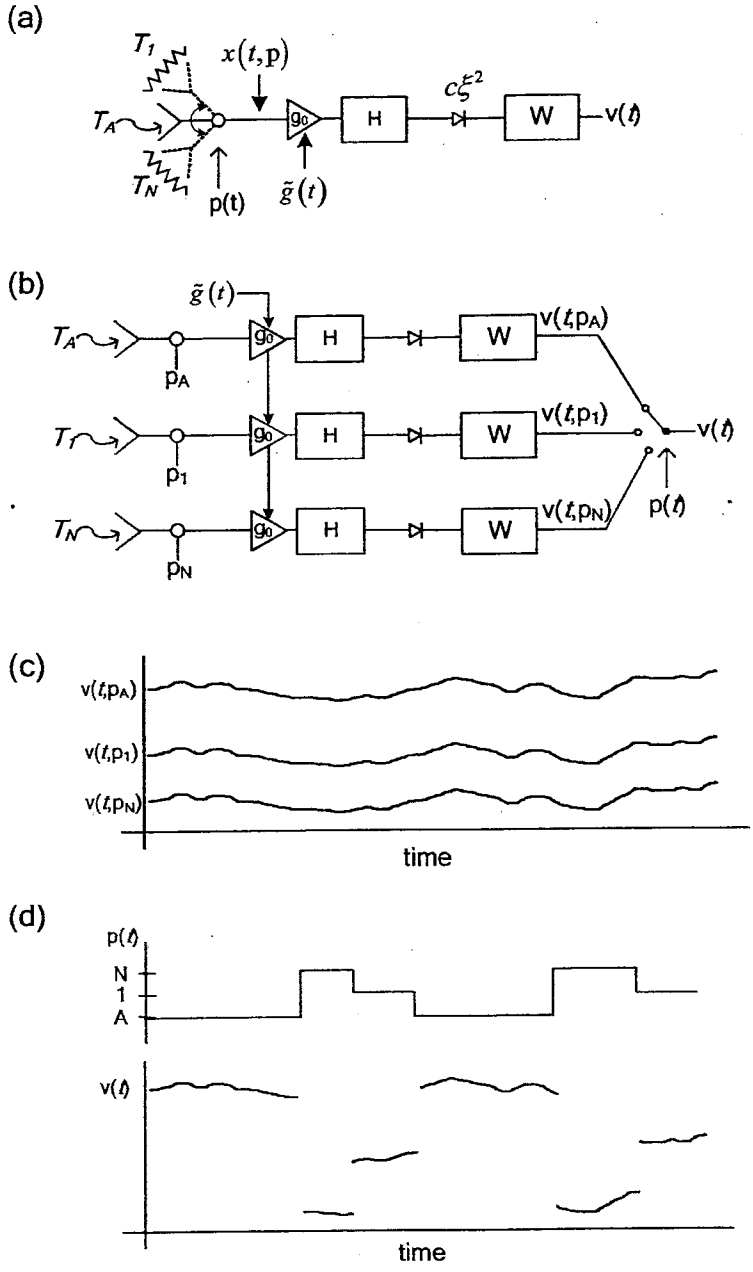


Figure 4: (a) A model of a radiometer with a switch used to view one of N + 1 radiation sources. The switch position is controlled by p(t). (b) The radiometer is expanded as a set of subsystems with each subsystem representing a different measurement path. (c) The signals out of the subsystems form a set of simultaneously existing random processes. (d) The radiometer output is a sequence of samples from the set of random processes.

**Figure 5**

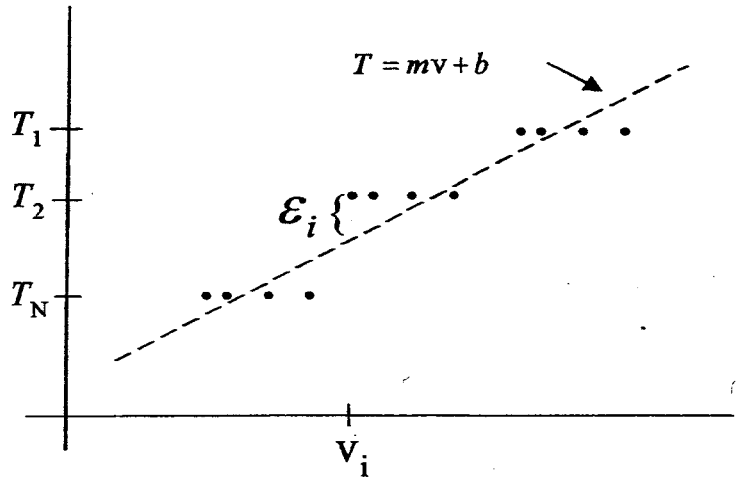


Figure 5: Graphical illustration of a calibration data set of $n$ measurements made at N different temperatures with $n > N$. The dashed line is the response of the radiometer.

**Figure 6**

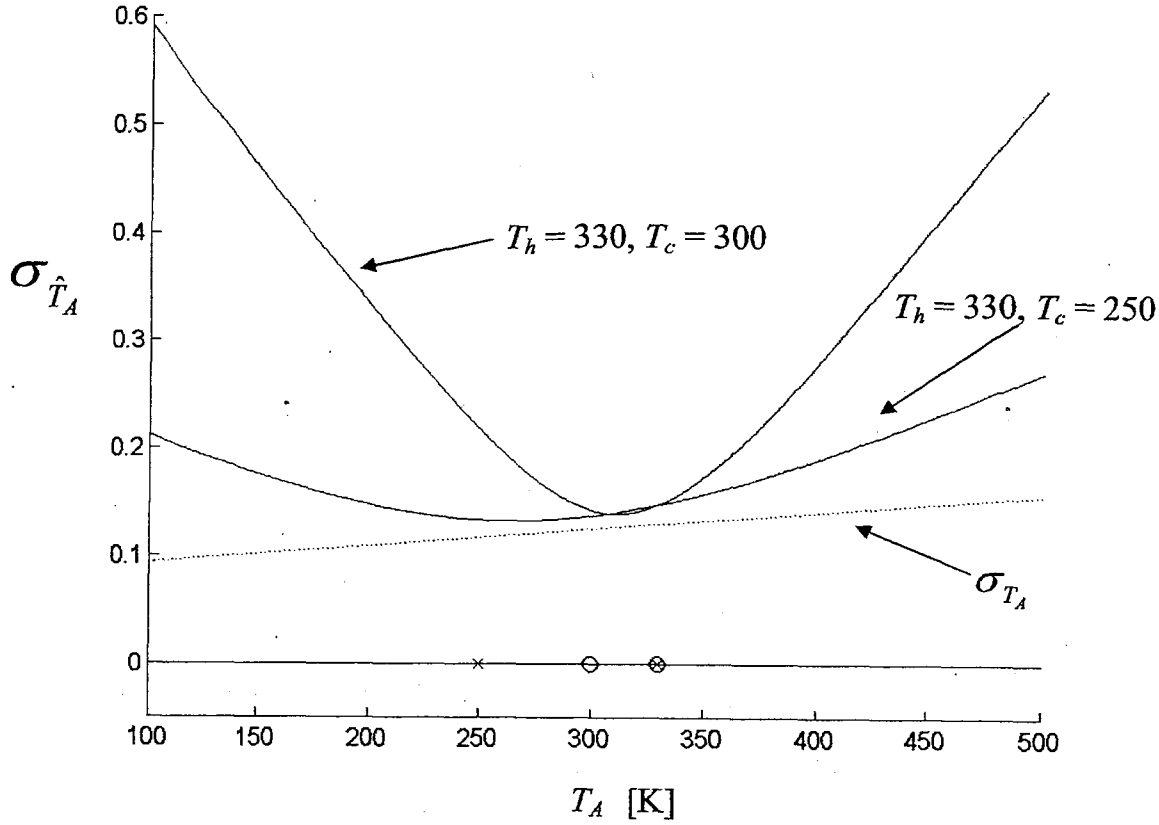


Figure 6: Standard measurement uncertainty versus measurand brightness temperature for two pairs of calibration target temperatures. The circles and x's on the abscissa indicate the temperatures of the calibration references. The dotted curve shows the resolution of the measurand observation.

**Figure 7**

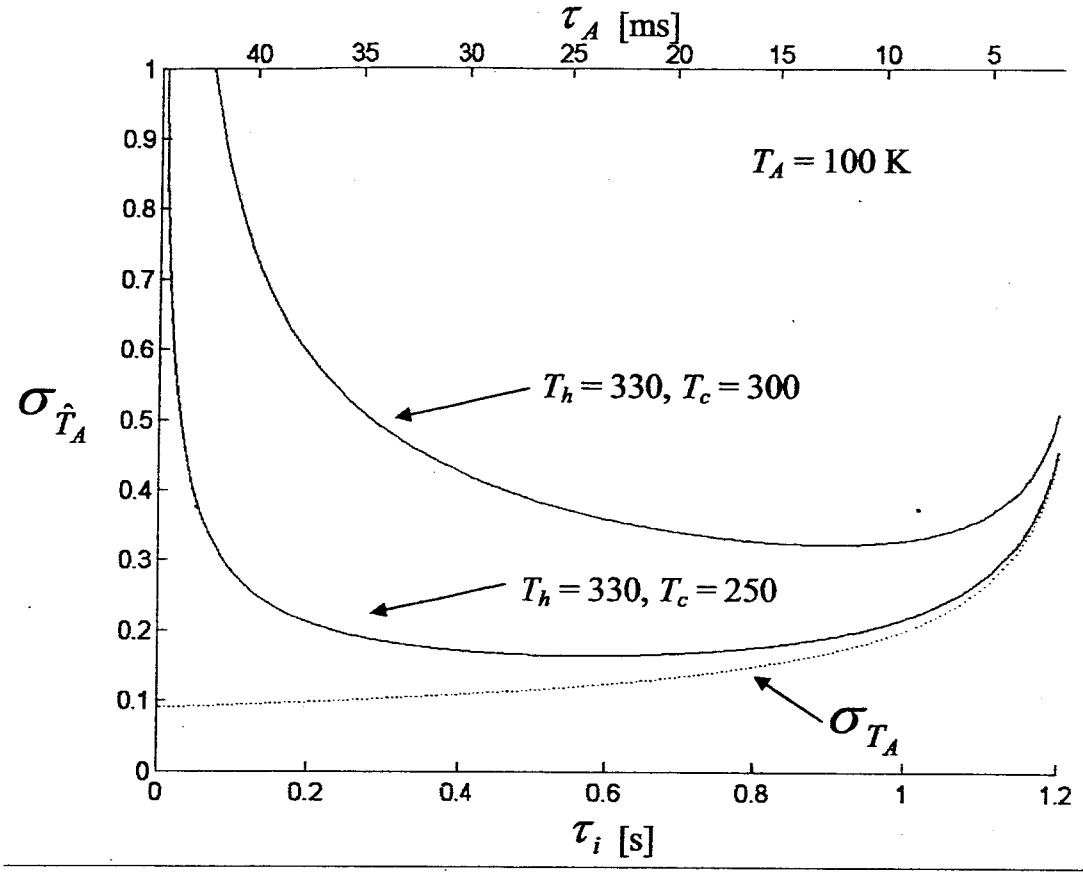


Figure 7: Standard measurement uncertainty as a function of time spent at each calibration reference (bottom abscissa) and time spent observing the measurand (top abscissa) for two pairs of calibration target temperatures. The dotted curve shows the resolution of the measurand observation.

**Figure 8**

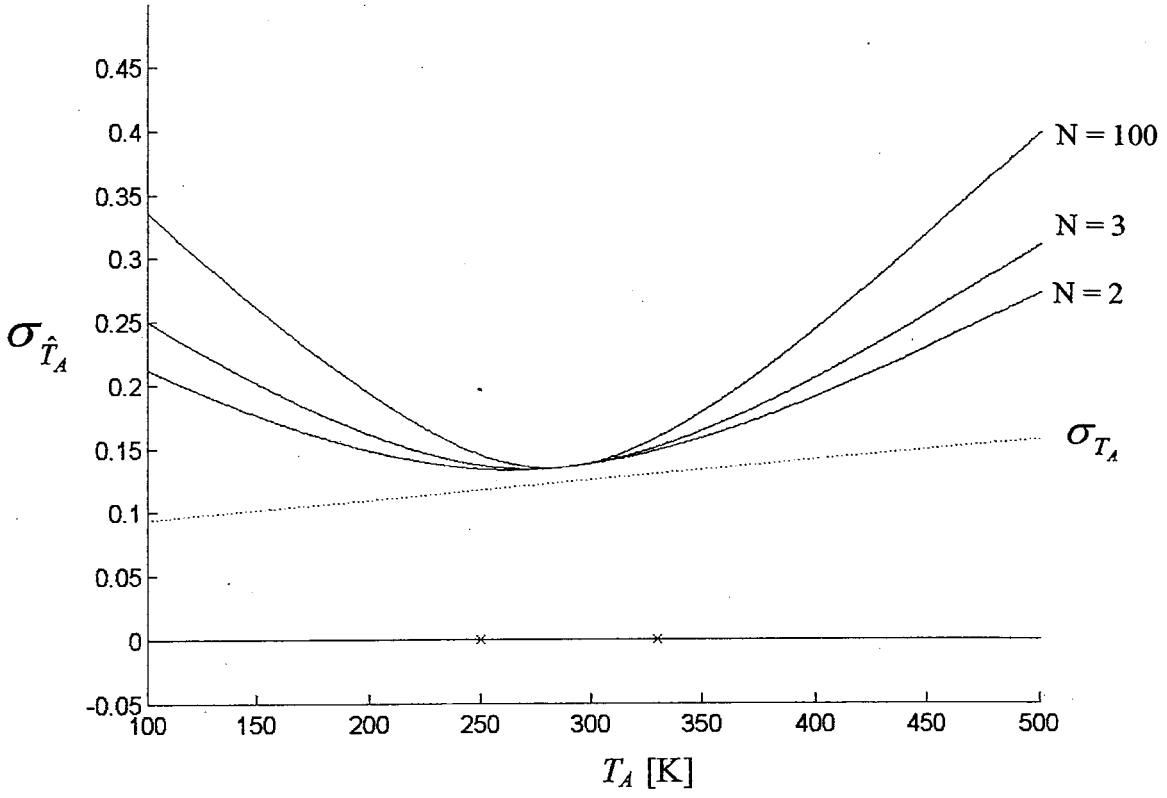


Figure 8: Standard measurement uncertainty as a function of measurand temperature for different numbers of reference temperatures used in the calibration. Reference temperatures are evenly distributed between 250 K and 330 K.

**Figure 9**

(a)

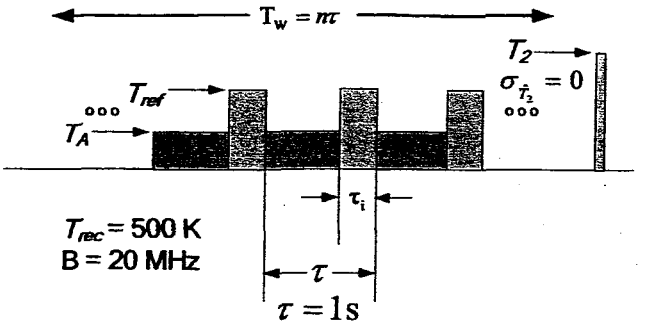


(b)

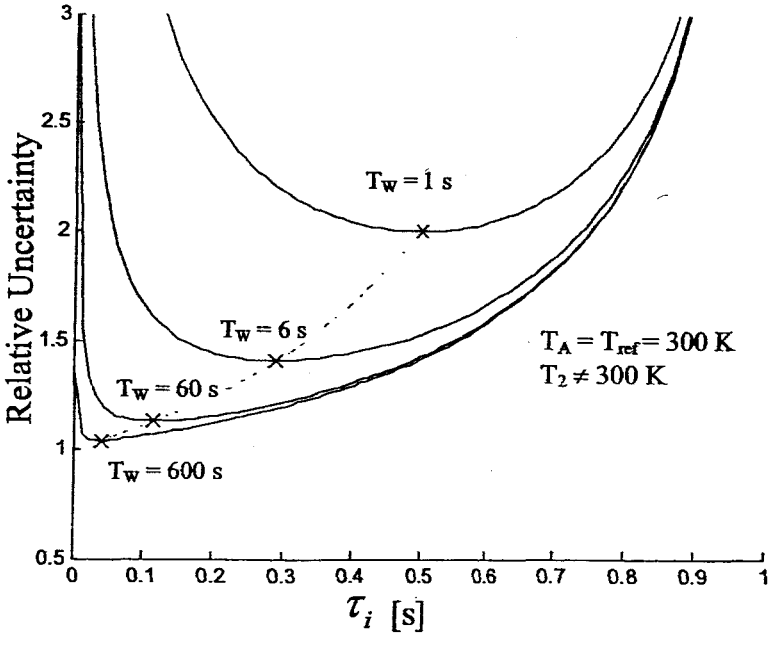


Figure 9: (a) A diagram of a time series of measurements from a single-reference switched radiometer. Reference-averaging is applied to the reference measurements over an interval $T_W$. A second reference, $T_2$, is observed with zero uncertainty outside the interval $T_W$. (b) The relationship between the reference-averaging window width, the reference integration time, and relative uncertainty is shown for the case when $T_{ref} = T_A = 300$ K. The dotted curve indicates the minimum as predicted by *Bremer* [1979].

**Figure 10**

**(a)**

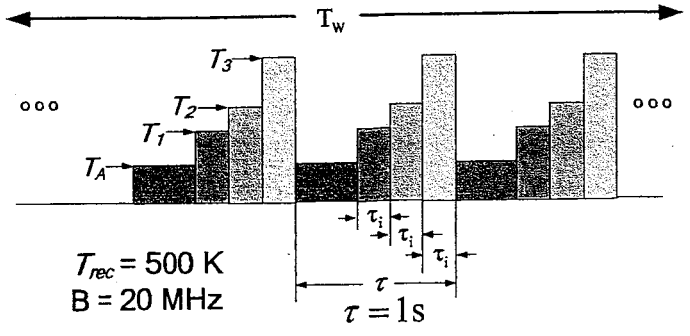


**(b)**

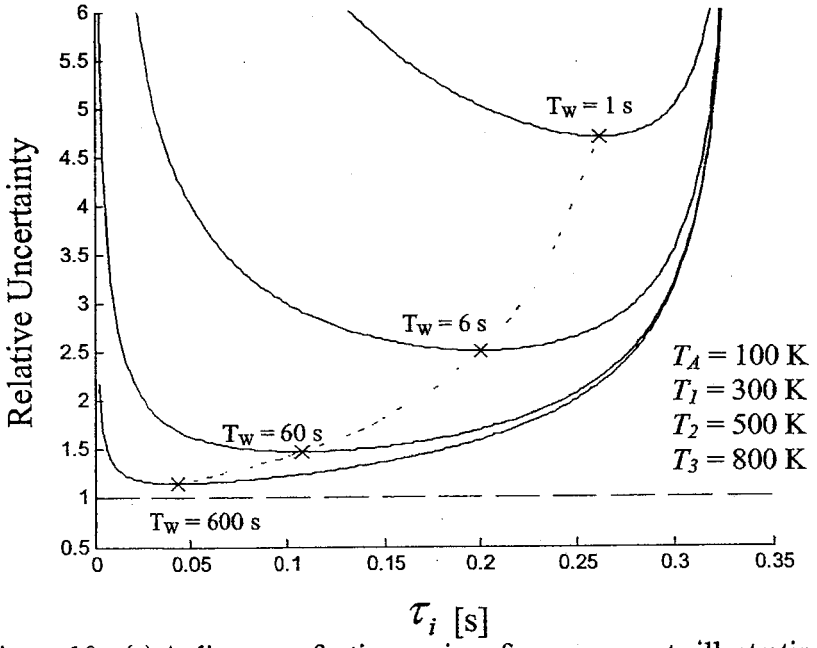


Figure 10: (a) A diagram of a time series of measurements illustrating a window over which reference-averaging is applied to the calibration measurements. (b) The relationship between the reference-averaging window width, the calibration reference integration time, and relative uncertainty. The dotted curve is the minimum relative uncertainty calculated over a range of $T_W$.